FI SEVIER

Contents lists available at ScienceDirect

# Science of the Total Environment

journal homepage: www.elsevier.com/locate/scitotenv



# Responses of soil moisture to climate variability and livestock grazing in a semiarid Eurasian steppe



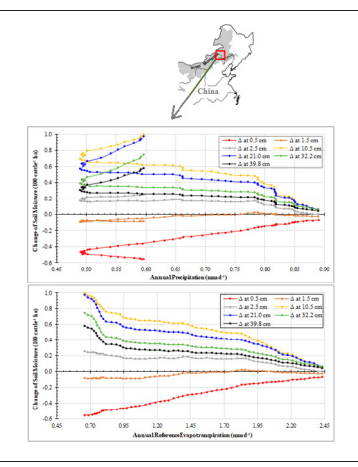
Xixi Wang <sup>a,\*</sup>, Ruizhong Gao <sup>b</sup>, Xiaomin Yang <sup>a</sup>

- <sup>a</sup> Department of Civil and Environmental Engineering, Old Dominion University, Norfolk, VA 23529-0241, USA
- b College of Water Conservancy and Civil Engineering, Inner Mongolia Agricultural University, 306 Zhaowuda Road, Hohhot, Inner Mongolia Autonomous Region 010018, China

#### HIGHLIGHTS

- A soil-water-plant-atmosphere model was parameterized for a semiarid steppe.
- The soil moistures varied 0.02 to 0.38, pulsing in spring and plateauing in summer.
- The optimal grazing intensity was determined to be around 3.0 cattle ha<sup>-1</sup>.
- The grazing impacts on soil moisture decreased with increase of evapotranspiration.

#### GRAPHICAL ABSTRACT



## ARTICLE INFO

Article history: Received 20 January 2021 Received in revised form 14 March 2021 Accepted 19 March 2021 Available online 25 March 2021

Editor: José Virgílio Cruz

Keywords: Climate change Ecohydrological modeling Soil water SWAP Wind erosion

## ABSTRACT

Soil water is vital for sustaining semiarid ecosystems. However, data on soil moisture have unlikely been continuously collected for a long time (e.g., >50 years), let alone under various combinations of climates and livestock grazing intensities. The objective of this study was to formulate and parameterize an ecohydrological model for predicting long-term variability of soil moisture, taking a typical Eurasian grassland located in northeast China as the testbed. The parameters were determined by extensive literature review, field reconnaissance, laboratory analyses of soil and grass samples, and model calibration using daily soil temperatures and soil moistures measured at four depths from 2014 to 2017. The model, driven by the daily climate data from 1955 to 2017, performed well in reproducing the measurements. Across the assessment years of 1960 to 2017, the daily soil moistures were predicted to vary from 0.02 to 0.38. Overall, the soil moistures at a shallower depth were smaller but had a wider range than those at a deeper depth, with a largest mean and a widest range around the 30 cm depth. Regardless of the depths, the soil moistures pulsed in beginning March and plateaued from May to September. Livestock grazing was precited to reduce top 1.5-cm soil moistures but increase moistures of the beneath soils. The optimal grazing intensity was determined to be around 3.0 cattle ha<sup>-1</sup>, above which wind erosion would become a concern. The grazing impacts on soil moisture were found to monophonically decrease with increase of evapotranspiration or annual precipitation of larger than 220 mm. For the years with an annual precipitation of less than 220 mm, such grazing impacts either increased or decreased with increase of precipitation, depending on the relative magnitude of evapotranspiration. Climate change will diminish soil moisture pulses in early spring, likely intensifying soil erosion by wind.

Published by Elsevier B.V.

<sup>\*</sup> Corresponding author. E-mail address: x4wang@odu.edu (X. Wang).

#### 1. Introduction

Soil moisture, the volumetric percentage of soil pores occupied by water, indicates the availability of water for sustaining fragile vegetation ecosystems in semiarid regions, including the Eurasian steppe grasslands (Singh et al., 1998; Kurc and Small, 2007), where the annual precipitation is less than 600 mm and the annual potential evapotranspiration (PET) can be higher than 1200 mm (Luo et al., 2014; Yang, 2014). For such ecosystems, most precipitation events can only wet the shallow soil layers for a short period of time, as the small amount of water evaporates quickly. Soil moistures control dynamics of water and carbon fluxes as well as physiological processes of respiration and assimilation. Herein, the respiration releases carbon dioxide ( $CO_2$ ) to the atmosphere by soil microorganisms and plants, whereas the assimilation fixes  $CO_2$  from the ambient atmosphere by plant photosynthesis. The difference between the released and fixed  $CO_2$  is the net ecosystem exchange (NEE), which is a determinant of plant biomass.

Previous studies (Singh et al., 1998; Huxman et al., 2004) have indicated that respiration and assimilation are positively related with actual evaporation and transpiration, respectively, and that NEE tends to increase with increase of soil moisture and vice versa. In semiarid environments, the respiration depends on top (i.e., 0 to 5 cm) soil moisture, most of which is lost to evaporation, the assimilation, on the other hand, depends on rootzone soil moisture, most of which is lost to transpiration. As a result, the response of NEE to precipitation fluctuation and subsequent soil wetting, water redistributing, and soil drying can be complex and very dynamic. The interannual variabilities of evaporation and transpiration increase with decrease of precipitation, possibly shifting a semiarid ecosystem from a carbon source in a wet year to a carbon sink in a dry year. Moreover, for a semiarid steppe grassland, the grazing intensity and timing can also influence evapotranspiration and soil moisture, and thus affect the NEE interactively with precipitation (Wang et al., 2020). Thus, a complete understanding of how soil moistures at variable depths respond to climate variations and grazing practices in a long run is imperative but currently lacking for sustaining semiarid steppe ecosystems.

Singh et al. (1998) conducted a field study along the topo-sequences of upland, midland, and lowland at the Central Plains Experimental Range, a shortgrass steppe grassland located in north-central Colorado, USA. The semiarid grassland receives an average annual precipitation of about 350 mm. For each of the top-sequence, four sites, which were predominantly covered by C<sub>4</sub> perennial bunchgrass (Bouteloua gracilis), were instrumented to monitor soil moisture at five (i.e., 30, 45, 60, 75, and 90 cm) depths and measure aboveground net primary production (ANPP) from 1985 to 1991. In terms of the U.S. Department of Agriculture (USDA) soil taxonomy (Saxton and Rawls, 2006), the soils were classified as sandy loam at one site, clay loam at second site, and sandy clay loam at other two sites. Regardless of the topo-sequences, the ANPP was found to be positively related with annual precipitation but inversely related with moistures of below-30-cm soils (i.e., deeper layers). These seemingly conflict relationships can be attributed to that the root density distribution disproportionated with the soil moisture profile: the roots in the above-30-cm soils (i.e., shallower layer) accounted for more than 80% of the total root biomass. A higher soil moisture in the deeper layers indicated that more infiltrated water from precipitation might not be able to be held in the shallower layer due to the very permeable loamy soils, resulting in somewhat water stress on the plants. The soil water in the shallower layer can be more efficiently transpired by the rich roots, and thus play a more important role in increasing ANPP, than that in the deeper layers (Luo et al., 2014; Pedram et al., 2018). The water in the deeper soil layers can buffer the impact of temporal variability in precipitation to at most stabilize the steppe grasses (Wang et al., 2016).

Kurc and Small (2007) instrumented a grassland of Sevilleta National Wildlife Refuge located in central New Mexico, USA. The semiarid grassland, which receives an average annual precipitation of 230 mm, has sandy soils; and its vegetation cover was dominated by C<sub>4</sub> perennial black grama (Bouteloua eriopoda). From 1 June 2002 to 1 January 2005, data on climate (i.e., precipitation, air temperature, solar radiation, and wind speed) and abiotic variables (i.e., soil moisture, soil temperature, heat flux, and carbon flux) were recorded continuously using a datalogger at a 15- or 30-min time interval. The soil moisture and temperature were measured at the 2.5, 12.5, 22.5, 37.5, and 52.5 cm depths, while the heat flux was observed at the 5 cm depth. In addition, a vertical profile distribution of the grass roots was determined by digging a trench near the measurement site to the rootzone bottom; and the profile distribution was empirically assumed to be invariant throughout the entire monitoring period: the roots in the top 40-cm soil layer accounted for more than 70% of the total root biomass, with the remaining roots stretching downward into the beneath deeper (i.e., 40- to 100-cm) soil layers. The data revealed that soil moisture pulses at the 2.5 cm depth following almost all rain events, whereas only four soil moisture pulses were observed at the 53.5 cm depth following either large precipitation events or a series of smaller events. The soil water in the top 15 cm layer was mainly evaporated and affected respiration, while the soil water in the below-15-cm layer was mostly transpired and controlled assimilation. An inverse relationship between NEE and evapotranspiration was observed, indicating that for the highly permeable sandy soils, the infiltrated water was able to travel downward into the below-15-cm layer rather than quickly evaporated from the surface soils.

Wang et al. (2020) examined effects of grazing regimes (i.e., intensities and seasons) on soil respiration using data collected in 2010 and 2011 at Loess Plateau Grassland Ecosystem Trial Station located in Gansu Province, northwest China. The station has sandy free-drainage loess soils and is a typical temperate steppe grassland with dominant species of Stipa bungeana, Lespedeza davurica, Pennisetum flaccidum, Artemisia capillaris, and Stetarua viridis. In 2001, two sites of 6 ha each that are comparable in terms of topography, physiography, and physiology were selected for controlled grazing experiments. For a given year between 2001 and 2010, one site was grazed in the warm season (i.e., June to September) for 90 days, whereas another site was grazed in the cold season (i.e., mid-November to late December) for 48 days. Each site was subdivided into twelve plots of 0.5 ha each, every three of which were treated as one group, leading to four groups with grazing intensities of 0.0, 2.7, 5.4, and 8.7 sheep ha<sup>-1</sup>, respectively. The grazing wether sheep had a live weight of 25  $\pm$  1.3 kg to minimize possible influences of livestock themselves. In May, September, and December of 2010 and 2011, besides 30-min interval precipitations, data on soil respiration, soil temperature and moisture, ANPP, and belowground net primary production (BNPP) were measured as well. The results indicated that for a given grazing season, a higher grazing intensity tended to result in smaller values of ANPP and BNPP but higher moistures of the top 1.0 cm soils and thus larger soil respirations, and vice versa. However, such causal relationships could be compounded by interannual variations of precipitation, air temperature, and radiation.

Existing studies, including those cited above, indicated needs and current knowledge limitations of how climate and livestock grazing interactively affect water and carbon cycles in semiarid steppe grasslands. Because those cycles are regulated by soil moisture dynamics, the objective of this study was to simulate the long-term variability of soil moisture profiles as affected by climatic fluctuations and grazing practices. The testbed was the Balagaer River watershed, a typical Eurasian steppe located in northeast Inner Mongolia Autonomous Region (IMAR) of China. The simulation was carried out for historical (i.e., 1955 to 2017) climates and four representative grazing regimes. It was expected to augment the existing knowledge and information in sustaining semiarid grasslands as an important carbon sink to confront climate change (Neumann and Wigen, 2013).

## 2. Modeling framework

#### 2.1. Governing equations

In semiarid environments, water and heat transports in unsaturated soil layers can be well approximated as one-dimensional vertical fluxes (Wang, 2015; Pedram et al., 2018). These two physical transport processes are coupled by soil-water properties, namely soil texture, moisture, and temperature.

For a given vertical soil column, the water transport process through a soil horizon is governed by the one-dimensional Richards equation (Charbeneau, 2000) expressed as:

$$\frac{\partial \theta}{\partial t} = \frac{\partial}{\partial z} \left[ K(\psi) \left( \frac{\partial \psi}{\partial z} + 1 \right) \right] - S_a(\psi) - S_d(\psi) - S_m(\psi) \tag{1} \label{eq:delta-theta-t$$

where  $\theta$  [—] is the soil moisture at time t [d]; z [cm] is the vertical coordinate taken zero on the ground surface and positively upward;  $\psi$  [cm] is the soil matric capillary potential head taken negatively for unsaturated soils and positively for saturated soils; K [cm d<sup>-1</sup>] is the unsaturated hydraulic conductivity;  $S_a$  [d<sup>-1</sup>] is the soil water extraction rate by plant roots;  $S_d$  [d<sup>-1</sup>] is the drainage rate from saturated soils; and  $S_m$  [d<sup>-1</sup>] is the water exchange rate with soil macro pores.  $S_a$  is always positive, whereas  $S_d$  and  $S_m$  are positive when the soil horizon functions as a water source but negative when the soil horizon as a water sink. The detailed discussions on  $S_d$  and  $S_m$  can be found in Kroes et al. (2017) and many other publications.

The heat transport process through this same soil horizon can be approximated by the one-dimensional convection equation (Philip and de Vries, 1957, Vanderborght et al., 2017) expressed as:

$$C_{sh}\frac{\partial T}{\partial t} = \frac{\partial}{\partial z} \left( \lambda_{sh} \frac{\partial T}{\partial z} \right) \tag{2}$$

where T [°C] is the soil temperature at time t [d];  $C_{sh}$  [J cm<sup>-3</sup> °C<sup>-1</sup>] is the apparent soil heat capacity; and  $\lambda_{sh}$  [J cm<sup>-1</sup> °C<sup>-1</sup> d<sup>-1</sup>] is the apparent soil thermal conductivity.  $C_{sh}$  and  $\lambda_{sh}$  are slightly larger than the corresponding real values to account for the heat diffusion by pore water vapor.

C<sub>sh</sub> can be estimated as the volumetric fractions-weighted average of heat capacities of the components, including sand particles (0.05 to 2.0 mm), silt particles (0.002 to 0.05 mm), clay particles (<0.002 mm), soil water, and pore air including vapor (de Vries, 1963). The volumetric fractions should be determined by excluding particles that are coarser than 2.0 mm and their summation must be equal to one. Herein, the volumetric fraction of water is equal to soil moisture, and the volumetric fraction of air is the difference between soil porosity (i.e., saturated soil moisture) and actual soil moisture. The heat capacities for sand, silt, clay, water, and air have been well documented to be 2.128, 2.496, 2.385, 4.180, and 0.001212 J cm $^{-3}$  °C $^{-1}$ , respectively. Similarly,  $\lambda_{sh}$ can be estimated as the weighted average of the component thermal conductivities for sand (7603 J cm<sup>-1</sup> °C<sup>-1</sup> d<sup>-1</sup>), silt (216 J cm<sup>-1</sup> °C<sup>-1</sup>  $d^{-1}$ ), clay (2523 J cm<sup>-1</sup> °C<sup>-1</sup>  $d^{-1}$ ), water (492 J cm<sup>-1</sup> °C<sup>-1</sup>  $d^{-1}$ ), and air. The weight for a component is the multiplication of its volumetric fraction and shape factor that reflects the sizes, shapes, and spatial arrangements of the component particles (Hillel, 1980). The typical values for the shape factors can be found in Ashby et al. (1996).

## 2.2. Unsaturated hydraulic conductivity

To solve Eq. (1),  $\psi$  and  $\theta$  need to be related by a retention curve of the soil. While various forms of functions have been proposed and used to define such a curve (Charbeneau, 2000), the modified van Genuchten function (Schaap and van Genuchten, 2006) has proven to be best suited for large-scale vadose zone flow and transport simulations and thus was adopted in this study. This function can be expressed as:

$$\Theta(\psi) = \frac{\theta(\psi) - \theta_r}{\theta_s - \theta_r} = \begin{cases} \left(1 + \left|\alpha\psi\right|^n\right)^{-m} & \psi \leq \psi_b \\ 1 & \psi > \psi_b \end{cases} \tag{3}$$

$$\alpha = \frac{\zeta}{|\psi_{\mathbf{b}}|} \tag{4}$$

$$n = \lambda + 1 \tag{5}$$

$$m = 1 - \frac{1}{n} \tag{6}$$

where  $\Theta(\psi)$  [-] is the effective saturation at capillary potential  $\psi$  [cm];  $\zeta$  [-] is a soil hysteresis factor taken different values for the main drying and wetting retention curves (Hillel, 1980);  $\theta_r$  [-] is the residual soil moisture;  $\theta_s$  [-] is the saturated soil moisture;  $\psi_b$  [cm] is the air-entry potential head; and  $\lambda$  [-] is the pore-size distribution index (van Genuvhten, 1980; Charbeneau, 2000).

Substituting Eq. (3) into the permeability model developed by Mualem (1976), the Mualem-van Genuchten formula for  $K(\psi)$  can be derived as:

$$K(\psi) = \begin{cases} K_s[\Theta(\psi)]^{\beta} \left[ \frac{1 - \left(1 - [\Theta(\psi)]^{\frac{1}{m}}\right)^m}{1 - \left(1 - [\Theta(\psi_b)]^{\frac{1}{m}}\right)^m} \right]^2 & \psi \leq \psi_b \\ K_s & \psi > \psi_b \end{cases}$$
 (7)

where  $K_s$  [cm  $d^{-1}$ ] is the saturated hydraulic conductivity; and  $\beta$  [-] is an empirical pore-connectivity parameter between -25 and 25 (Ashby et al., 1996).

The reduction impact of frost soil temperature on  $K(\psi)$  can be assumed to follow a linear function between two thresholds: one is the lowest soil temperature,  $T_1$ , below which soil water starts freezing, whereas another is the highest soil temperature,  $T_2$ , above which soil ice starts melting and below which all soil water except for residual water is frozen. That is, the hydraulic conductivity is equal to  $K(\psi)$  at  $T_1$  and zero at  $T_2$ , and for a soil temperature  $T_1$ , it can be estimated as:

$$K\prime(\psi) = \begin{cases} K(\psi) & T \geq T_1 \\ K(\psi) \frac{T - T_2}{T_1 - T_2} & T_2 < T < T_1 \\ 0 & T \leq T_2 \end{cases}$$
 (8)

## 2.3. Perennial grass growth and transpiration

Based on the crop models presented by van Ittersum et al. (2003), a computer program called WOFOST was developed in 1988 (Boogaard et al., 2014). Since then, WOFOST has been gone through several upgrading versions resulting from its world-wide applications to simulate various agricultural crop systems (Ma et al., 2011, de Wit et al., 2012, Cheng et al., 2016, Hack-ten Broeke et al., 2016). WOFOST simulates physiological processes of respiration, assimilation, and organ growing and deceasing to estimate crop yields, subject to field management practices (e.g., irrigation, fertilization, and pesticide control) for alleviating water and nutrient stresses. The WOFOST algorithms might be adapted to model perennial grass systems by using the forcing functions as a function of Julian day number instead of crop development stage as well as by relating root dry matter with rooting depth (Kroes et al., 2017). Mowing or grazing practices can be triggered either by a minimum amount of aboveground dry matter or a fixed date. For grazing, the consumed biomass depends on the relation between livestock intensity, grazing days, biomass consumption, and dry matter loss due to manure droppings and treading. The dynamics of leave area index (LAI), stem biomass, and root depth and density can be predicted using corresponding assimilation partitioning functions as a function of Julian day number.

The potential soil water extraction rate at depth z by plant roots,  $S_{p,z}$  in cm  $d^{-1}$ , is computed as:

$$S_{p,z} = \frac{\xi(z)}{\int_{-d_c}^{0} \xi(z)} T_p \eqno(9)$$

where  $\xi(z)$  [cm<sup>-2</sup>] is the root density, the ratio of root length to inclusive soil volume, at soil depth z [cm];  $d_{\xi}$  [cm] is the grass rootzone thickness; and  $T_p$  [cm d<sup>-1</sup>] is the potential transpiration rate.

The actual soil water extraction at depth z,  $S_a(\psi)$  in cm  $d^{-1}$ , is computed as:

$$S_{a}(\psi) = \alpha_{d}\alpha_{o}\alpha_{s}S_{p,z} \tag{10} \label{eq:10}$$

where  $\alpha_d$  [-],  $\alpha_o$  [-], and  $\alpha_s$  [-] are the reduction factors due to drought, oxygen, and salinity stress, respectively.  $\alpha_d$  can be estimated using the formulas presented by Feddes et al. (1978) or de Jong van Lier et al. (2008);  $\alpha_o$  by Feddes et al. (1978) or Bartholomeus et al. (2008); and  $\alpha_s$  by Maas and Hoffman (1977).

The average actual soil water extraction rate from the rootzone,  $T_a$  ( $\psi$ ) in cm  $d^{-1}$ , can be computed as:

$$T_a(\psi) = \frac{\int_{-d_\xi}^0 S_a(\psi) dz}{d_\xi} \eqno(11)$$

## 2.4. Computer program

Kroes et al. (2017) developed an integrated Soil-Water-Atmosphere-Plant (SWAP) computer program to solve Eqs. (1) and (2) simultaneously using a finite-difference approach. In this regard, the terms in those two equations are determined by Eqs. (3) to (11) and other formulas embedded in the program. A soil column of interest is subdivided into several sublayers, each of which should be homogeneous in terms of texture and soil-water properties; and in turn, each sublayer can be further discretized into a number of compartments with a smaller thickness to best mimic heat and water dynamics. Driven by climate time series, SWAP continuously simulates the state variables such as  $\theta(\psi)$  in terms of specified parameters of management practices (e.g., grazing), physiography, and physiology. This study used SWAP 4.0.1A, which was created and provided by Kroes (2020) after fixing a bug of the grass growth module.

SWAP uses a water balance module to calculate water storage change in a ground-surface ponding reservoir. The influxes into the reservoir include throughfall, irrigation, snowmelt, runon, floodwater, and discharge from (or seepage into) the topmost compartment, whereas the effluxes out of the reservoir include evaporation, surface runoff, and water exchange with macropores. The surface runoff occurs when the water storage in the reservoir exceeds its maximum capacity and can be computed as the ratio of an exponential function of the difference of storage and capacity to a resistance parameter for the reservoir attenuation effects. In addition, SWAP estimates the interflow from a saturated compartment as an exponential function of the difference between the shallow groundwater level and the hydraulic head of the drain. Further, the direct runoff is computed as the summation of surface runoff and interflows from all saturated compartments. Moreover, SWAP uses either the Penman-Monteith method (Penman, 1948; Monteith, 1965) or an empirical reference evapotranspiration approach (Allen et al., 1989, Allen et al., 1998) to determine PET. The actual evaporation is equal to PET if the reservoir is not empty and estimated as the upward Darcy flux out of the topmost compartment if the reservoir is dry. Precipitation is treated as rainfall when air temperature is above a threshold or snowfall when air temperature is below another threshold, and as mixture of thereof when air temperature is between these two thresholds. A temperature-based approach (Wang and Melesse, 2005) is used to model snowpack accumulation and snowmelt. The throughfall is computed as the difference of rainfall and interception, which is estimated as a function of LAI (Wang et al., 2012). In the SWAP's finite-difference scheme, the ponding reservoir is taken as the upper boundary.

## 3. Materials and methods

## 3.1. The study site

The study site was articulated to represent the overall characteristics of the 5365 km<sup>2</sup> Balagaer River watershed (Fig. 1), a mid-latitude Eurasian steppe grassland located in northeast IMAR. The watershed is almost uniformly covered by two perennial rhizome grass species, namely *Stipa grandis* and *Leymus chinensis* (Chen et al., 2005, Wang et al., 2014). Based on the authors' field reconnaissance in Julies of 2011 and 2012, the grasses had an average population density of about 4500 m<sup>-2</sup>, a mean individual height of 20 cm, a maximum root depth of 40 cm, and a mean individual diameter of 0.1 cm. The grass growing season is from late April to early October, during which livestock (i.e., sheep and cattle) graze from late May to late September (Shiyomi et al., 2011). The altitudes of the watershed vary from 857 to 1876 m, leading to a mean topographic gradient of 0.07.

In July 2012, the authors took and analyzed soil samples from 70 sites randomly positioned across the watershed (Fig. 1). Our visualizations of the field sampling trenches indicated two soil layers: the upper layer is from ground surface to a 30 cm depth, while the lower layer is from the 30 to 100 cm depth. Thus, for a given site, using a 6cm-diameter 3-cm-tall auger, three samples were taken within the upper layer, while another three samples were taken within the lower layer. Each of the samples was carefully put into a labeled plastic bag, which was quickly zipped and placed into a portable cooler to be subsequently transported back to our laboratory for analyses. Averaged across the watershed, the soils consist of 72 to 76% sand particles, about 23% silt particles, and 2 to 3% clay particles (Fig. 2a), and thus can be classified as sand or sandy loam according to the USDA soil texture triangle (Saxton and Rawls, 2006). The textures of the lowerlayer soils have a larger variation than those of the upper-layer soils probably due to the soil geomorphic history of the Mongolia Plateau (Luo et al., 2012). This is further verified by the larger mean coefficient of uniformity  $(C_u)$  and coefficient of curvature  $(C_c)$  for the lower-layer soils (Fig. 2b). C<sub>11</sub> is the ratio of 60%- to 10%-finer diameters, whereas C<sub>c</sub> is the ratio of 30%-finer diameter squared to the multiplication of 10%- and 60%-finer diameters (Charbeneau, 2000). The lower-layer soils can be more permeable than the upper-layer soils at one site but less permeable at another site, as indicated by the varying saturated hydraulic conductivities. As expected, the upper-layer soils have overall larger values for saturated soil moisture and field capacity than the lower-layer soils (Fig. 2c). Moreover, our field surveys of the 100 domestic wells (Fig. 1) and interviews of the pastures reveal that the depths to water table are larger than 3.0 m across the watershed except for some low-lying areas in the vicinity of streams and intermittent ponds.

The watershed receives 170 to 615 mm precipitation annually, with a mean of 335 mm. Most of the precipitation falls between July and September as rain and between October and January as snow. However, the watershed has an annual PET of 1165 mm or higher, which is much greater than the mean annual precipitation. Thus, the watershed has a semiarid climatic condition. The annual mean daily average air temperature is 1.2 °C, with a maximum daily air temperature of up to 37.5 °C in summer and a minimum daily temperature of as low as -38.5 °C in winter. The watershed has an annual mean daily average wind speed of about 15 km h $^{-1}$  and can have 28 to 148 windy days for a given year. For a given windy day, the maximum wind speed can reach as high as 125 km h $^{-1}$ . The annual mean discharge at the watershed outlet is 0.33 m $^3$  s $^{-1}$ , which is equivalent to an average annual runoff depth of 1.9 mm (i.e., runoff coefficient of less than 0.005). This indicates that the

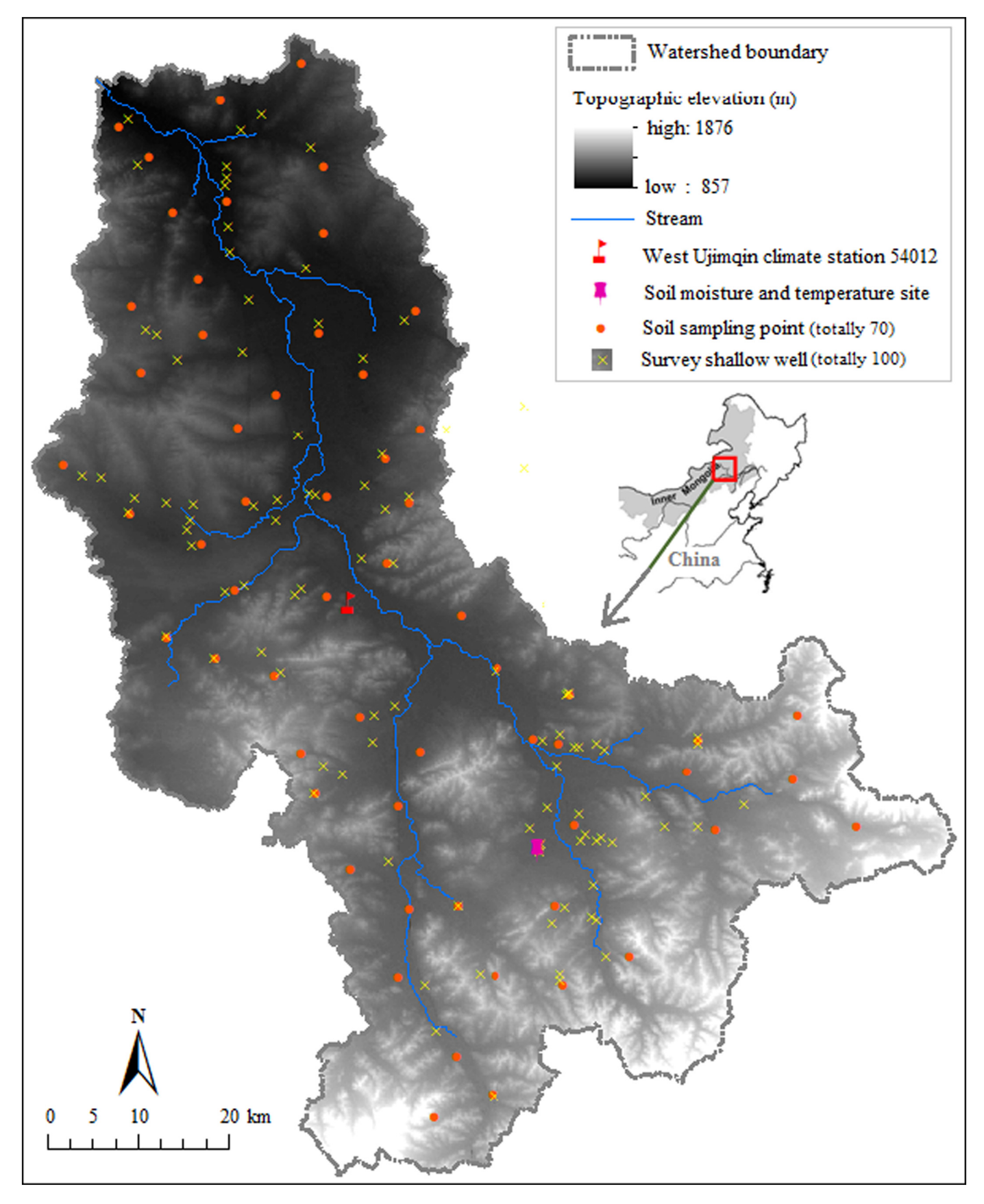


Fig. 1. The Balagaer River watershed and its topography; superimposed by the observation and survey points where data were used in this study.

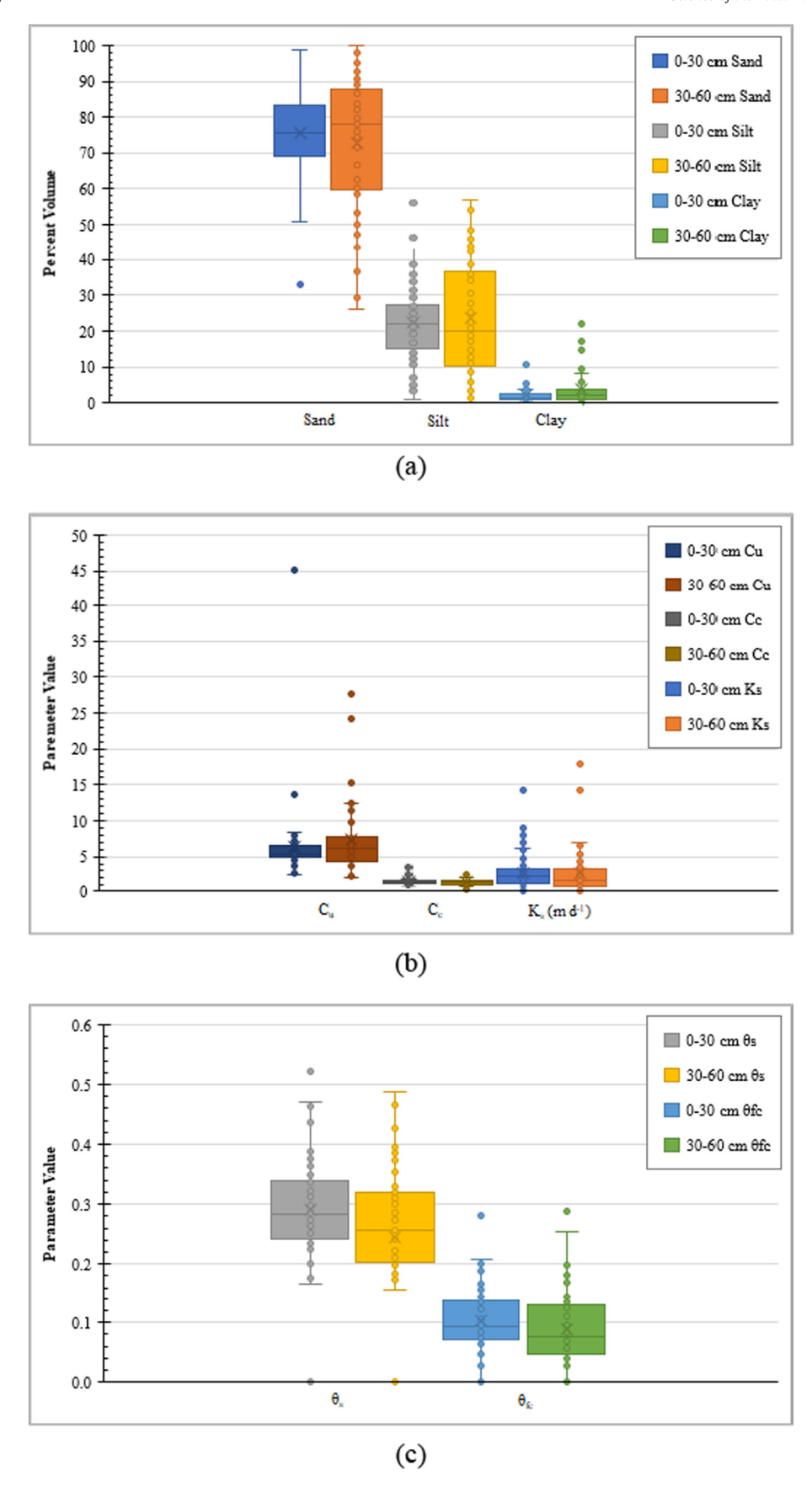


Fig. 2. Box-Whisker plots of the soil textures and soil-water properties.  $C_u$ : coefficient of uniformity;  $C_c$ : coefficient of curvature;  $K_s$ : saturated hydraulic conductivity;  $\theta_s$ : saturated soil moisture;  $\theta_{fc}$ : field capacity.

hydrologic cycle of the watershed is dominated by vertical rather than horizontal water movements and can be well modeled using SWAP. The primary water users are agriculture, animal husbandry, domestic, and power industry.

## 3.2. Data and preprocessing

Besides our surveyed soil data mentioned above, daily data on precipitation, air temperature, relative humidity, wind speed, solar radiation, and reference evapotranspiration at West Ujimqin Climate Station 54012 (117°36′ E, 44°35′ N) were obtained from Chinese Meteorological Information Center (CMIC, 2020) for the record period of 1 January 1955 to 31 December 2017. In addition, at the soil moisture and temperature site (117°52′ E, 44°20′ N), four EC-5 three-needle sensors (METER Group, 2020) were installed at 5, 10, 15, and 30 cm depths, respectively, to continuously measure soil moisture and temperature from 2014 to 2017, and the measurements were recorded using a Campbell® Scientific CR3000 datalogger at an 12-h time interval. The sensors have a detection range of zero to one at an accuracy of  $\pm 1\%$  for soil moisture and a measurement range of -40 to 50 °C at an

accuracy of  $\pm 0.3$  °C. On a given day, four pairs of soil moisture and temperature were recorded around 0:00 am (i.e., at nighttime) and another four pairs around 12:00 pm (i.e., at daytime). For a given depth, the soil moisture and soil temperature of this day were computed as the arithmetic averages of the corresponding two diurnal values. Due to disconnections of the cables between the sensors and datalogger by livestock, the measurements for some days were lost. The complete (i.e., nomissing) records were available from 31 May to 31 December 2014, 1 January to 31 December 2015, 1 January to 10 May 2016, 30 August to 31 December 2016, and 1 January to 5 March 2017.

Further, the authors conducted an extensive literature review and did reconnaissance and laboratory analyses to estimate the physiologic parameters (Table 1) for *Stipa grandis* and *Leymus chinensis* (Wang and Zhou, 2012). Because these two grass species intermingle (Luo et al., 2014) and share a number of common features (Chen et al., 2005), the estimated parameters were assumed to characterize a hybrid rather either of these two species. When taking the soil samples in July 2012, the authors also measured root densities at various soil depths. Based on our measurements and literature data (Kurc and Small, 2007; Pereyra et al., 2017), this study developed and used the functional relationship

**Table 1**The literature and estimated physiologic parameters for a hybrid of *Stipa grandis* and *Leymus chinensis*.

Class (source)	Parameter	Description	Possible range <sup>a</sup>	Value	
Initialization (authors)	LAIEM [m <sup>2</sup> m <sup>-2</sup> ]	Leaf area index (LAI) at emergence	0-10	0.01	
	RGRLAI $[m^2 m^{-2} d^{-1}]$	LAI increasing rate per day	0-1	0.1	
Surface area (authors)	SSA [ha kg <sup>-1</sup> ]	Specific stem area	0-1	0.0004	
	SPAN [d]	Optimum life span of leaves	0-366	30	
	TBASE [°C]	Lowest temperature for leaves to grow	-10-30	0	
	SLA [ha kg <sup>-1</sup> ]	Specific leave area	0-1	0.0015-0.00	
Assimilation (Wang and Zhou, 2012)	KDIF	Extinction coefficient for diffuse visible light	0-2	0.6	
	KDIR	Extinction coefficient for direct visible light	0-2	0.75	
	EFF [kg ha <sup>-1</sup> h <sup>-1</sup> $W^{-1}$ m <sup>2</sup> ]	Light use efficiency	0–10	0.5	
	AMAX [kg $ha^{-1} h^{-1}$ ]	Maximum CO <sub>2</sub> assimilation rate	0-100	25-40	
Conversion (Wang and Zhou, 2012)	CVL [kg kg <sup>-1</sup> ]	Efficiency of conversion into leaves	0-1	0.685	
	CVR [kg kg <sup>-1</sup> ]	Efficiency of conversion into roots	0-1	0.694	
	CVL [kg kg <sup>-1</sup> ]	Efficiency of conversion into stems	0-1	0.662	
Respiration (Wang et al., 2016)	Q10 [°C <sup>-1</sup> ]	Respiration rate increase with temperature	0-0.5	0.2	
	RML [kg $CH_2O kg^{-1}$ $d^{-1}$ ]	Maintenance respiration rate of leaves	0–1	0.03	
	RMR [kg CH <sub>2</sub> O kg <sup>-1</sup> $d^{-1}$ ]	Maintenance respiration rate of roots	0–1	0.015	
	RMS [kg CH <sub>2</sub> O kg <sup>-1</sup> d <sup>-1</sup> ]	Maintenance respiration rate of stems	0-1	0.015	
Partitioning (Wang and Zhou, 2012)	FRTB [kg kg <sup>-1</sup> ]	Fraction of total dry matter partitioned to roots	0-1	0.3	
	FLTB [kg kg <sup>-1</sup> ]	Fraction of aboveground dry matter partitioned to leaves	0-1	0.6	
	FSTB [kg kg <sup>-1</sup> ]	Fraction of aboveground dry matter partitioned to stems	0-1	0.4	
Death rate (Wang and Zhou, 2012)	PERDL [kg kg <sup>-1</sup> d <sup>-1</sup> ]	Maximum relative death rate of leaves due to water stress	0-3	0.05	
	RDRRTB [kg kg <sup>-1</sup> d <sup>-1</sup> ]	Maximum relative death rate of roots	0-3	0.02	
	RDRSTB [kg kg <sup>-1</sup> d <sup>-1</sup> ]	Maximum relative death rate of stems	0-3	0.02	
Oxygen stress (Feddes et al., 1978; Chen et al., 2005; Kroes	HLIM1 [cm]	Potential head above which no water extraction	-100-100	-2	
et al., 2017)	HLIM2U [cm]	Potential head above which optimum water extraction starts for top layer	-100-100	-16.1	
	HLIM2L [cm]	Potential head above which optimum water extraction starts for sub layer	-100-100	-44.4	
Drought stress (Feddes et al., 1978; Chen et al., 2005; Kroes et al., 2017)	HLIM3H [cm]	Potential head below which water uptake reduction at high Tpot	<100	-44.4	
ct al., 2017)	HLIM3L [cm]	Potential head below which water uptake reduction at low Toot	<100	-81.2	
	HLIM4 [cm]	Potential head below which no water extraction	<100	-170.7	
	ADCRH [cm d <sup>-1</sup> ]	Level of high atmospheric demand	0-5	5	
	ADCRL [cm d <sup>-1</sup> ]	Level of low atmospheric demand	0-5	5	
	ALPHACRIT [-]	Critical stress index for compensation of root water uptake	0.2-1	0.95	
Interception (authors)	COFAB [cm]	Maximum interception amount	0-1	0.01	
Root growth (authors)	RDI [cm]	Initial rooting depth	>0	20	
	RRI [cm $d^{-1}$ ]	Maximum daily increase in rooting depth	>0	0.01	
	RDC [cm]	Maximum rooting depth of grass cultivar	>0	40	
	WRTMAX [kg DM ha <sup>-1</sup> ]	Maximum root dry mass	>0	20,000	

<sup>&</sup>lt;sup>a</sup> Source: Kroes et al. (2017).



Fig. 3. The synthetic root density distribution for a hybrid of Stipa grandis and Leymus chinensis.

between relative root density and relative rooting depth as shown in Fig. 3. Herein, at a root depth of interest, the relative root density is the ratio of the root density at this depth to the maximum root density of the whole rootzone, while the relative rooting depth is the ratio of this depth to the rootzone thickness (i.e., 40 cm).

Moreover, the authors reviewed a variety of documents from the local governments and interviewed several herders, leading to the summary grazing information in Table 2. On a yearly basis between 1985 and 2017, the 19,700-ha focal area within the Balagaer River watershed was grazed by 100,000 to 260,000 cows and horses and at the same time by 800,000 to 1,700,000 sheep and goats. Based on the formula presented by USDA-NRCS (2020) and in reference to cattle, the animal unit equivalent (AUE) was computed as 233,333 to 543,333, which is equivalent to grazing intensities ranging from 11.8 to 27.6 cattle ha<sup>-1</sup>, with an average of 19.7 cattle  $ha^{-1}$ . The livestock might start grazing once the aboveground dry matter is more than 350 kg  $ha^{-1}$ , with the after-grazing dry matter of less than 150 kg ha<sup>-1</sup> and a dropping and treading loss of 0.43 to 0.5 kg ha<sup>-1</sup>. According to AHDB (2020), the dry matter consumption per AUE was estimated to be 8.5 to 10.0 kg ha<sup>-1</sup>; the higher the actual grazing intensity, the smaller the consumption rate, and vice versa. The study grassland was ever and never irrigated, fertilized, and mowed.

## 3.3. Model setup and parameterization

A 200-cm-long soil column was subdivided into four sublayers with thicknesses of 20, 10, 30, and 140 cm, respectively, in the downward direction. The first or third sublayer was subdivided into 20 compartments, while the second sublayer was subdivided into 5 compartments and the fourth sublayer into 14 compartments. The compartments of a given sublayer have a same thickness, which is computed as the division of the sublayer thickness by the number of compartments. For instance,

**Table 2** The grazing intensity from 1985 to 2017.<sup>a</sup>

Statistics	Number of cattle and horse	Number of sheep	AUE (cattle) <sup>b</sup>	Grazing area (ha)	Grazing intensity (cattle ha <sup>-1</sup> )		
Min	100,000	800,000	233,333	19,700	11.8		
Max	260,000	1,700,000	543,333	19,700	27.6		
Average	180,000	1,250,000	388,333	19,700	19.7		

<sup>&</sup>lt;sup>a</sup> In general, the grazing season is from May 20 to September 30.

each of the 20 compartments of the first sublayer is 1.0 cm thick, whereas each of the 14 compartments of the fourth sublayer is 10.0 cm thick. The first and second sublayers belong to the upper (i.e. 0 to 30 cm) layer and the third sublayer corresponds to the lower (i.e., 30 to 60 cm) layer. The fourth sublayer can be considered as the deeper layer. The soils of the lower and deeper layers were assumed to have same soil-water properties, as evidenced by Wang et al. (2014) and authors' visual examinations of several well-digging cores. The initial values for the soil-water parameters in Eqs. (3) to (7), namely  $\theta_r$ ,  $\theta_s$ ,  $K_s$ ,  $\alpha$ , n, and  $\beta$ , were determined in terms of our measurements (Fig. 2) and literature data for sand and sandy loam soils (Charbeneau, 2000). These parameters along with others (Table 3) were automatically adjusted using PEST (Parameter Estimation) (Doherty, 2004, Wang et al., 2008) to make simulated soil moistures and temperatures closely match the corresponding observations from 2014 to 2017. PEST is a model-independent parameter estimator with advanced predictive analysis and regularization features. The upper boundary condition was defined by the observed air temperatures and the lower boundary condition was specified as free drainage because of the large depth to water table. The physiological parameters listed in Table 1 were used to parameterize the grass growth module of the SWAP

The model performance was measured using visualization plots and three statistics, namely coefficient of determination ( $R^2$ ), Nash-Sutcliffe efficiency ( $R_{\rm ns}$ ), and mean absolute error (MAE). The detailed formulizations of these statistics can be found in Wang and Melesse (2005).  $R^2$  is the proportion of the variance in observations that can be explained by the model; its value can range from zero to 1.0. As a rule of thumb, a larger  $R^2$  indicates a better model performance. The value of  $R_{\rm ns}$  can range from  $-\infty$  to 1.0, with higher values indicating a better overall fit and 1.0 indicating a perfect fit. A negative  $R_{\rm ns}$  indicates that the simulation results are less reliable than if one had used the average of the observed values, while a positive value indicates that the simulation results are more reliable than using this average. MAE measures errors between paired values expressing the same phenomenon and is computed as an arithmetic average of the absolute errors.

## 3.4. Simulation and assessment

The SWAP model was run from 1 January 1955 to 31 December 2017, during which the first five years were used as the warm-up period to stabilize the model parameters and the successive 58 years were

<sup>&</sup>lt;sup>b</sup> AUE: animal unit equivalent to cattle; AUE = number of cattle and horse + number of sheep/6 (AHDB, 2020; USDA-NRCS, 2020).

**Table 3**The calibrated parameters of the SWAP model.

Hydrologic process	Parameter	Description	Possible range <sup>a</sup>	Calibrated value		
Snow and frost TePrRain [°C]		Temperature above which all precipitation is rain	0–5	2.0		
	TePrSnow [°C]	Temperature below which all precipitation is snow	-5-0	0.0		
	SNOWCOEF [-]	Calibration factor for snowmelt	0-10	0.3		
Surface runoff	PONDMX [cm]	Maximum storage depth of ground-surface ponding reservoir	>0	0.01		
RSROEXP [-]	Exponent of water depth above PONDMX	0.1-10	1.0			
	RSRO [cm <sup>RSROEXP-1</sup> d]	Drainage resistance	<1	0.95		
Evapotranspiration	CF [ — ]	Adjustment factor of reference evapotranspiration	0-2	Fig. 4		
Soil water <sup>b</sup>	$\theta_{\rm r}$ [cm <sup>3</sup> cm <sup>-3</sup> ]	Residual soil moisture	0-0.4	UL: 0.02		
				LL: 0.02		
$\theta_s$ [cm <sup>3</sup> cm	$\theta_{\rm s}$ [cm <sup>3</sup> cm <sup>-3</sup> ]	Saturated soil moisture	0-0.95	UL: 0.35		
				LL: 0.40		
$K_s$ [	$K_s$ [cm d <sup>-1</sup> ]	Saturated vertical hydraulic conductivity	>0	UL: 286.98		
	$\begin{array}{c} \text{RSRO}\left[\text{cm}^{\hat{\kappa}\text{SR}\hat{o}\text{EXP-1}}d\right]\\ \text{RSRO}\left[\text{cm}^{\hat{\kappa}\text{SR}\hat{o}\text{EXP-1}}d\right]\\ \text{CF}\left[-\right]\\ \theta_{r}\left[\text{cm}^{3}\text{cm}^{-3}\right]\\ \theta_{s}\left[\text{cm}^{3}\text{cm}^{-3}\right]\\ K_{s}\left[\text{cm}d^{-1}\right]\\ \alpha\left[\text{cm}^{-1}\right]\\ n\left[-\right] \end{array}$			LL: 312.78		
α	$\alpha$ [cm <sup>-1</sup> ]	Retention curve shape factor (Eq. (4))	0.0001-1	UL: 0.05		
				LL: 0.05		
n [—]	n [—]	Retention curve shape factor (Eq. (5))	1-4	UL: 2.5		
				LL: 2.5		
β[	β[-]	Empirical pore-connectivity parameter (Eq. (7))	-25-25	UL: 2.5		
				LL: 2.5		
	ψ <sub>b</sub> [cm]	Air-entry potential head	<0	UL: −2.0		
				LL: −2.0		

<sup>&</sup>lt;sup>a</sup> Source: Kroes et al. (2017).

taken for assessments. Multiple model runs were executed: the first run used the average AUE grazing intensity of 19.7 cattle ha<sup>-1</sup> for model calibration and was considered as the baseline condition, whereas the second and third runs assumed AUE grazing intensities of 0.0 and 27.6 cattle ha<sup>-1</sup>, respectively. Besides, more trial runs were executed by varying grazing intensities to determine the threshold above which further increasing intensity would not affect soil moisture anymore. Herein, the null hypothesis was that grazing influences would become minimal once the aboveground biomass was too small to be grazed. The purpose of using different grazing intensities was to assess both individual and interactive impacts of grazing and climate on soil moisture.

For a given grazing intensity, summary statistics, namely average, minimum, and maximum, of the simulated soil moistures at each depth were separately computed by grazing season (i.e., May 20 to September 30) and nongrazing season (i.e., October 1 to May 19) from 1 January 1960 to 31 December 2017. Subsequently, for the assessed grazing intensities, the profiles of paired statistics versus soil depth were created to virtually examine impacts of grazing intensity on soil moisture. In addition, for a given soil depth, the same statistics were computed at a daily time step throughout the 58 assessment years and plotted; these time-series plots were virtually compared with the corresponding plots of daily precipitation and reference ET to examine effects of climate variability on soil moisture. Further, the time-series plots were compared across the grazing intensities to scrutinize interactive effects of grazing intensity and climate variability, particularly for the depths with a relatively large grazing impact as revealed by the profile plots.

#### 4. Results

## 4.1. The calibrated SWAP model

For the snow and frost processes, the precipitation was in the form of rain when the air temperature was above 2.0 °C and in the form of snow when the air temperature was below 0.0 °C; between these two threshold temperatures was in a mixture of rain and snow (Table 3). The snowmelt factor, which controls the melting speed of snowpack, was determined to be 0.3. For the surface runoff process, the surface ponding reservoir had a maximum storage depth of 0.01 cm, above which surface runoff could be estimated as a linear function with a slope of about 1.053 d. For the soil water evapotranspiration and movement processes, the adjustment factors were determined to be 2.0 for winter

and 0.5 for other three seasons (Fig. 4). The saturated soil moisture and hydraulic conductivity for the lower soil layer were slightly larger than those for the upper soil layer, the other soil-water parameters, however, were same for both soil layers; this is consistent with the data shown in Fig. 2.

The SWAP model had an excellent performance in reproducing the measured daily soil temperatures regardless of the depths (Table 4). For the calibration periods, the prediction errors of the average daily mean temperatures ranged from -0.72 to 0.70 °C only, with a comparable scatteredness as indicated by the standard deviations. The model captured more than 75% of the variances presented in the observations and could trace the fluctuations of the observed temperatures ( $R_{ns}$  > 0.9). At a given depth, the observed soil temperatures from 1 January to 5 March 2017 were almost constant, making R<sub>ns</sub> a less appropriate statistics. The plots of predicted versus observed daily mean soil temperatures revealed a similar pattern regardless of the calibration periods. To be concise, the plots for 2015 are shown in Fig. 5 and those for other three years are not presented. On the other hand, the SWAP model well predicted the average daily mean soil moistures (Table 4), as indicated by the compatible standard deviations and small values of mean absolute errors (MAE < 0.04). Although the model could barely explain the variances presented in the observed daily mean soil moistures of 2014, 2015, and 2017 ( $R^2 < 0.3$ ), it fairly traced the overall fluctuation patterns of the observations in 2015 (Fig. 6) and other calibration years (not shown to be concise). The annual precipitation in 2014 was 363.0 mm, representing an above-average hydroclimatic condition, whereas the annual precipitations in 2016 and 2017 were 295.5 and 172.4 mm, respectively, representing the below-average hydroclimatic conditions. The annual precipitation in 2015 was 315.4 mm, which is close to the long-term average annual precipitation of 335 mm. Given that this study focused on long-term variations of soil moistures in response to climate variability and grazing regimes, the SWAP model was judged to be sufficiently calibrated.

#### 4.2. The simulated soil moistures

Across the assessment period of 1960 to 2017, for a given depth, the average soil moisture during the grazing season was higher than that during the nongrazing season; the intraday fluctuation of soil moistures, however, was much wider for the nongrazing than grazing season (Fig. 7). Throughout the soil column, regardless of the seasons, the average soil moisture tended to be higher at a deeper depth, approaching a

<sup>&</sup>lt;sup>b</sup> UL: upper (i.e., 0 to 30 cm) soil layer; LL: lower (i.e., below-30 cm) soil layer.

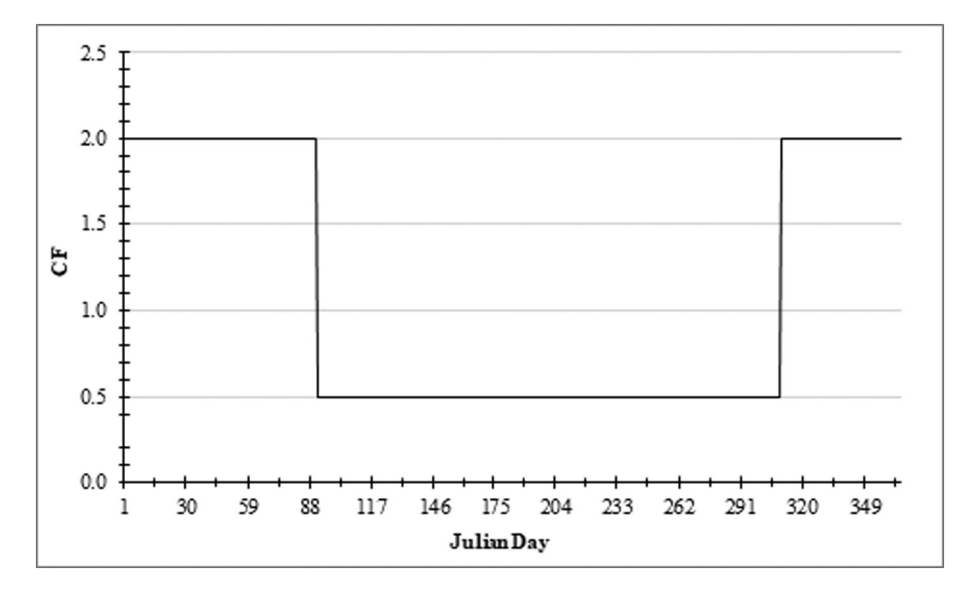


Fig. 4. The calibrated values of CF, adjustment factor for reference evapotranspiration.

constant. The moistures of the top 60-cm soils varied more widely than those of the beneath soils. The near-surface soils could be very wet on one day and become very dry on another day, with a highest soil moisture occurring around the 32 cm depth.

Regardless of the soil depths, the fluctuation patterns of the average daily mean soil moisture broadly synchronized with those of the average daily precipitation and average daily reference evapotranspiration, as illustrated by those for the 0.5 and 32.2 cm depths (Fig. 8). The average soil moistures at other depths might have different magnitudes but had similar fluctuation patterns; herein they are not shown to be concise. The average soil moistures were almost constant in January and February, pulsed between March and April, increased gradually in May, plateaued from late May to September, and decreased steadily from October onwards. However, for a given day in late February to beginning March, the soil moisture might vary largely from one year to

another, with the largest variability in coincidence with the pulsing peak. In contract, the soil moisture slightly varied interannually for a given day in April to September, moderately varied for a given day in October and November, and barely varied for a given day in December to mid-February. Such interannual variabilities of the daily soil moistures were dependent on the interannual variabilities of the daily precipitation and daily ET<sub>0</sub>: the large variability of precipitation of a given day in April to September was likely offset by the corresponding large variability of ET<sub>0</sub>, resulting in a smaller variability of the daily soil moistures during these six months than that in beginning March.

Grazing could slightly decrease the soil moistures in the top 1.5-cm soils but increase the soil moistures in the beneath soils (Fig. 7). If the grassland were not grazed, more days in February and March would have a relatively high soil moisture in the top 1.5-cm soils (e.g., Fig. 8e versus Fig. 8c) but fewer days in the beneath soils (e.g., Fig. 8f versus

**Table 4**The performance statistics of the SWAP model.<sup>a</sup>

Calibration period	Soil temperature			Soil moisture			Soil temperature			Soil moisture						
	Mean (°C)	Sd. (°C)	$R^2$	R <sub>ns</sub>	Mean	Sd.	MAE	R <sup>2</sup>	Mean (°C)	Sd. (°C)	$R^2$	R <sub>ns</sub>	Mean	Sd.	MAE	R <sup>2</sup>
	at 5 cm soil depth							at 10 cm soil depth								
May 31 to Dec. 31, 2014	7.83	13.15	0.97	0.95	0.10	0.04	0.03	0.15	7.87	12.77	0.97	0.96	0.10	0.04	0.03	0.09
	7.81	12.51			0.08	0.02			7.92	12.29			0.09	0.02		
Jan. 01 to Dec. 31, 2015	3.53	13.20	0.96	0.94	0.09	0.04	0.03	0.13	3.56	12.91	0.97	0.95	0.09	0.04	0.03	0.10
	3.21	13.13			0.07	0.02			3.19	12.97			0.08	0.02		
Jan. 01 to May 10, 2016	-7.19	10.65	0.91	0.85	0.07	0.03	0.04	0.84	-7.19	10.30	0.91	0.85	0.08	0.03	0.04	0.83
	-7.63	11.63			0.05	0.01			-7.89	11.22			0.06	0.02		
Aug. 30 to Dec. 31, 2016	-1.20	10.04	0.95	0.94	0.10	0.05	0.04	0.45	-0.77	9.82	0.96	0.94	0.11	0.05	0.04	0.46
	-0.69	10.46			0.08	0.02			-0.42	10.37			0.08	0.02		
Jan. 01 to Mar. 05, 2017	-15.21	3.06	0.76	0.33	0.05	0.00	0.02	0.36	-14.89	2.87	0.76	0.23	0.05	0.00	0.02	0.00
	-14.49	4.55			0.06	0.00			-14.48	4.25			0.07	0.00		
	at 15 cm soi	il depth							at 30 cm so	il depth						
May 31 to Dec. 31, 2014	7.83	12.29	0.97	0.96	0.09	0.03	0.03	0.05	7.91	10.99	0.98	0.97	0.10	0.04	0.03	0.08
	8.03	12.09			0.09	0.02			8.34	11.59			0.10	0.02		
Jan. 01 to Dec. 31, 2015	3.52	12.53	0.97	0.95	0.08	0.03	0.03	0.06	3.46	11.55	0.98	0.95	0.08	0.03	0.02	0.29
	3.18	12.83			0.08	0.02			3.19	12.54			0.09	0.01		
Jan. 01 to May 10, 2016	-7.20	9.89	0.92	0.84	0.07	0.03	0.04	0.83	-6.95	9.16	0.92	0.78	0.08	0.04	0.04	0.82
	-8.13	10.85			0.06	0.02			-8.58	10.15			0.08	0.01		
Aug. 30 to Dec. 31, 2016	-0.40	9.57	0.96	0.94	0.10	0.04	0.03	0.47	0.56	9.02	0.96	0.91	0.12	0.05	0.04	0.44
	-0.16	10.29			0.09	0.02			0.56	10.13			0.10	0.02		
Jan. 01 to Mar. 05, 2017	-14.58	2.68	0.75	0.10	0.05	0.00	0.03	0.27	-13.75	2.31	0.77	-0.48	0.06	0.00	0.02	0.00
	-14.48	3.99			0.07	0.00			-14.46	3.34			0.08	0.00		

<sup>&</sup>lt;sup>a</sup> S<sub>d</sub>.: standard deviation; R<sup>2</sup>: coefficient of determination; R<sub>ns</sub>: Nash-Sutcliffe efficiency; MAE: mean absolute error; the bold numbers are based on the daily measurements.

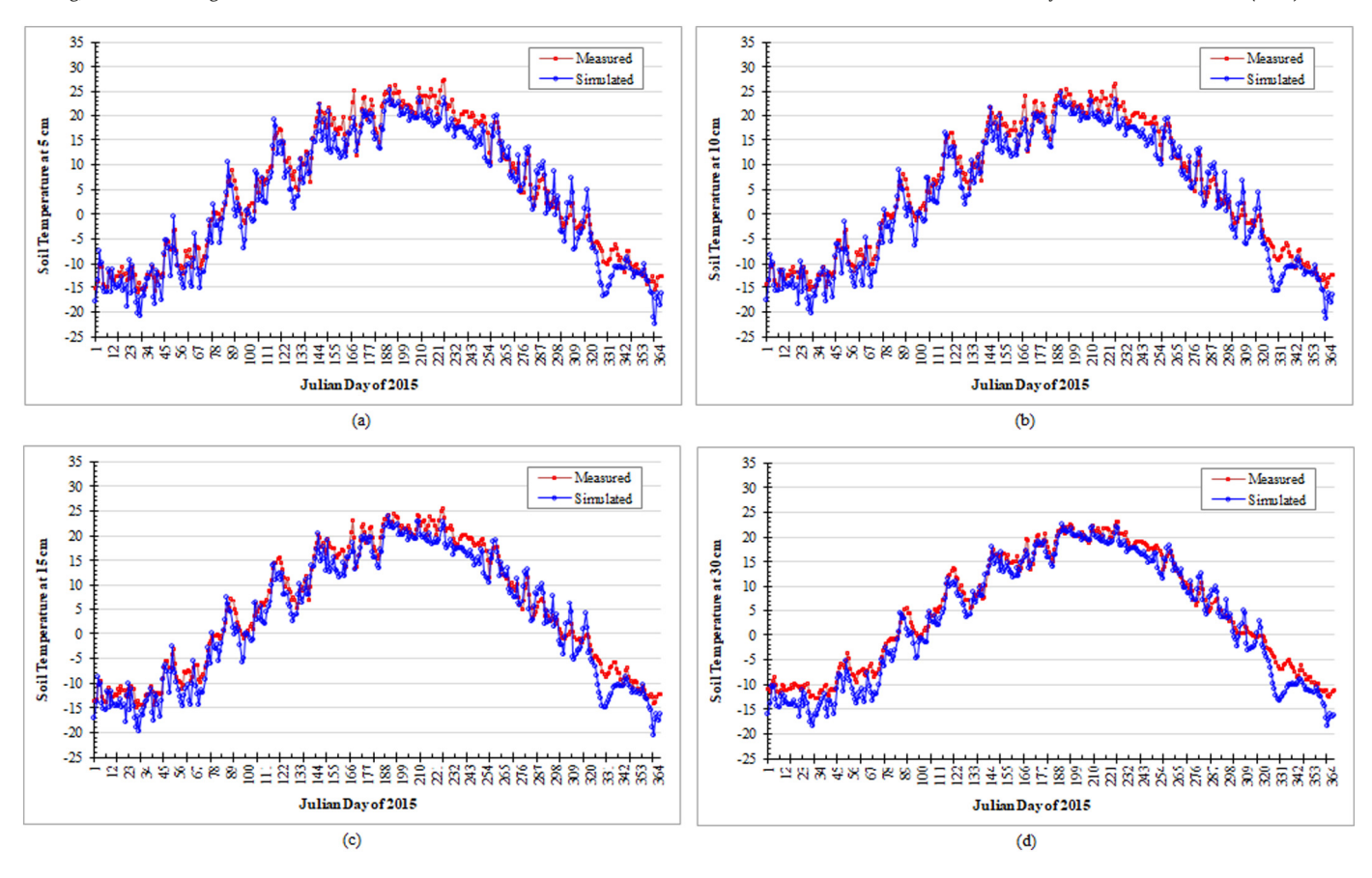


Fig. 5. The simulated versus measured daily mean soil temperatures in 2015 at below-ground depths of: (a) 5 cm; (b) 10 cm; (c) 15 cm; and (d) 30 cm.

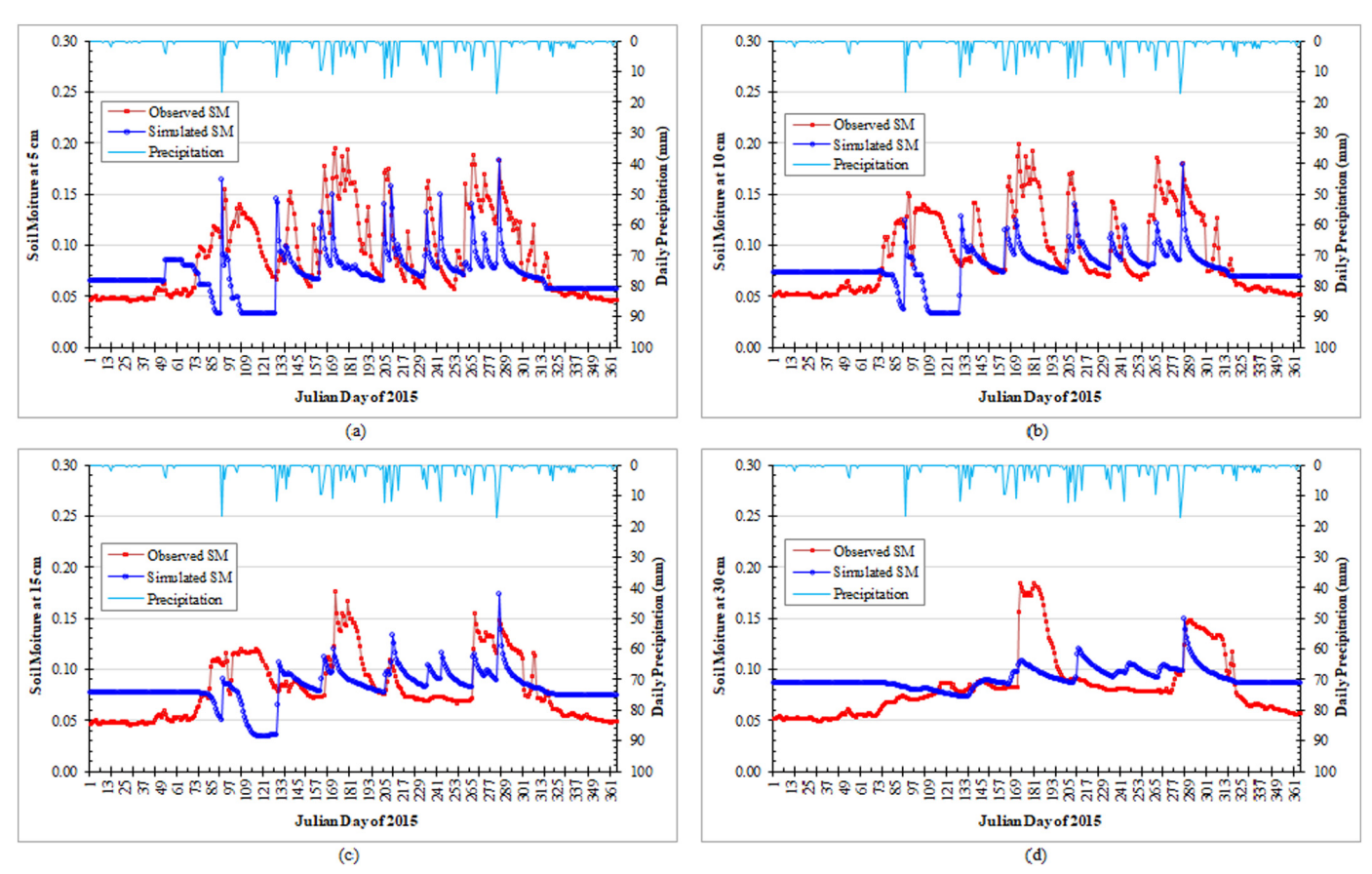
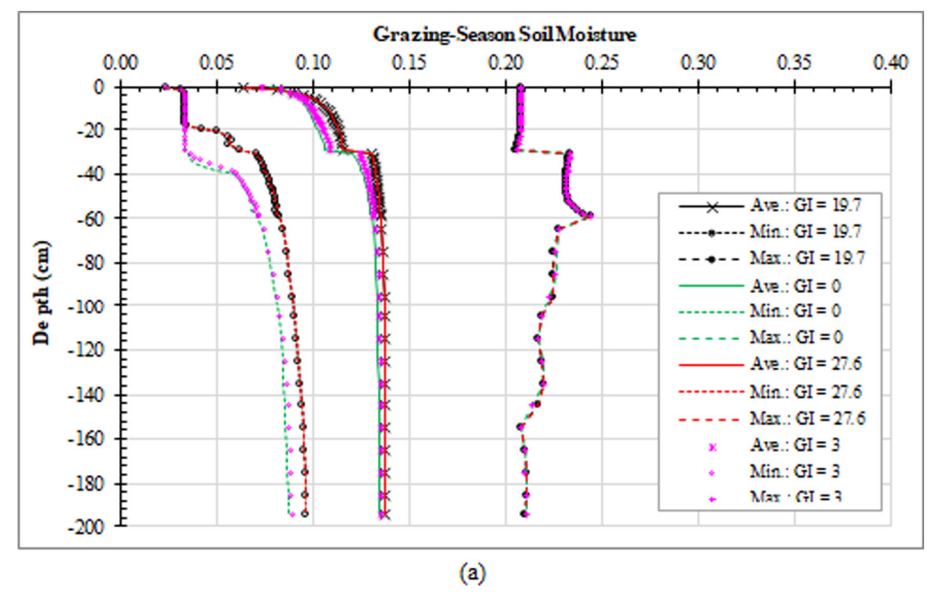
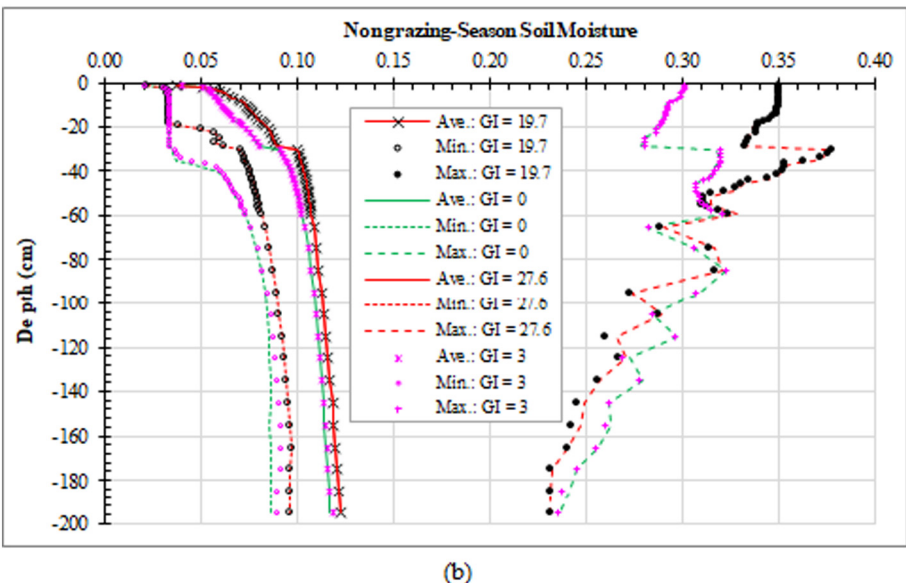


Fig. 6. The simulated versus measured daily mean soil moistures in 2015 at below-ground depths of: (a) 5 cm; (b) 10 cm; (c) 15 cm; and (d) 30 cm.





**Fig. 7.** Averages and ranges of the daily mean soil moistures from 1960 to 2017 for selected grazing intensities during: (a) grazing season (May 20 to September 30); and (b) nongrazing season (October 1 to May 19). Ave.: average; Min.: minimum; Max.: maximum; and GI: grazing intensity, in cattle ha<sup>-1</sup>.

Fig. 8d). Such a change in number of days because of grazing was not noticed in other ten months. Overall, grazing tended to reduce the interannual variability of soil moistures on a day of interest: the lower the grazing intensity, the smaller the variability, and vice versa. Correspondingly, grazing would reduce the maximum daily soil moisture by about 0.05 and have a near-zero influence on the minimum daily soil moisture. Such grazing influences were predicted to become negligible once the grazing intensity would be greater than 3.0 cattle ha<sup>-1</sup> (Fig. 8g and h), which is way lower than the current average grazing intensity of 19.7 cattle ha<sup>-1</sup>.

Regardless of the soil depths, the relationship between soil moisture change and precipitation was not unique when the annual precipitation was less than 220 mm (i.e., 220 mm/365 d = 0.6 mm d<sup>-1</sup>): the soil moisture change could either increase or decrease with increase of precipitation (Fig. 9a). However, when the annual precipitation was more than this threshold, the soil moisture change would monophonically decrease with increase of precipitation, approaching zero at a precipitation amount of about 0.9 mm d<sup>-1</sup>. In contrast, the soil moisture change was found to decrease persistently with increase of ET<sub>0</sub>, approaching zero at a reference evapotranspiration of about 2.5 mm d<sup>-1</sup> (Fig. 9b).

Moreover, because of grazing, the top 1.5-cm soils would become drier while the beneath soils tended to be wetter. The near-surface and around-10.5-cm soils could be mostly affected by grazing. For a grazing intensity of 4.0 cattle  $ha^{-1}$  or higher, the moistures of the top 0.5-cm soils would be reduced by up to 0.025 and the moistures of the around-10.5-cm soils would be increased by up to 0.04. For a year with an annual precipitation of less than 220 mm, the soil moisture change was interactively affected by precipitation, ET<sub>0</sub>, and grazing intensity, whereas for a year with an annual precipitation of larger than this threshold, the soil moisture change was interactively affected by precipitation and grazing intensity and seemed to be independent of ET<sub>0</sub>.

#### 5. Discussion

The SWAP model performed better in reproducing the measured soil temperatures than soil moistures. This is possibly because the measurement site is not co-located with climate station 54012, between which the straight-line distance is about 35 km (Fig. 1). In the common knowledge, the air temperature and solar radiation, which are major influencing factors for soil heat transport and soil temperature fluctuation, can

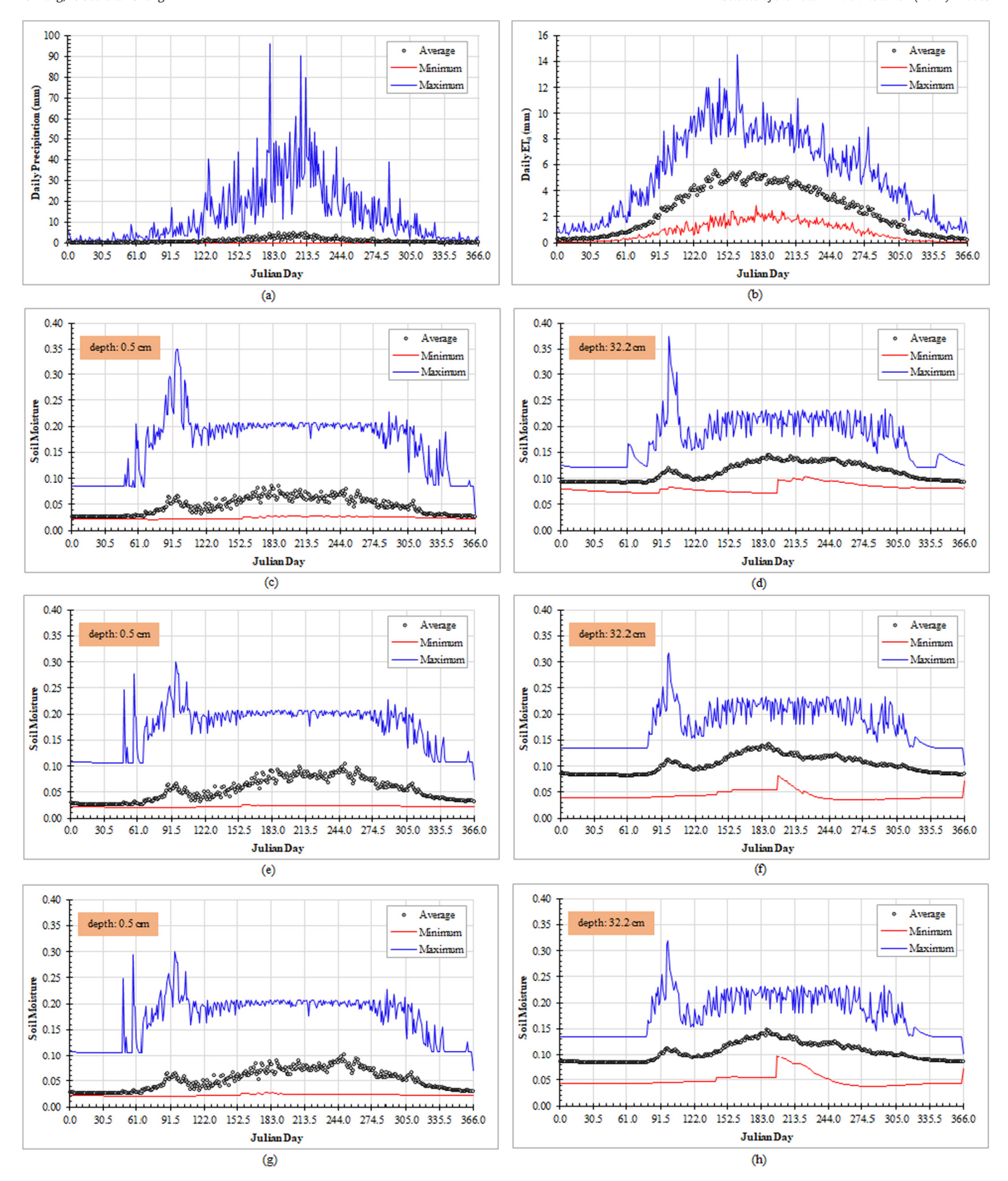


Fig. 8. Averages and ranges from 1960 to 2017 of the daily: (a) precipitation; (b) reference evapotranspiration,  $ET_0$ ; (c) and (d) soil moistures for grazing intensity GI = 19.7 cattle  $ha^{-1}$ . (e) and (f) soil moistures for GI = 0.0; and (g) and (h) soil moistures for GI = 3.0 cattle  $ha^{-1}$ . The soil moistures at 0.5 and 32.2 cm had largest fluctuations and are shown for explanation purposes.

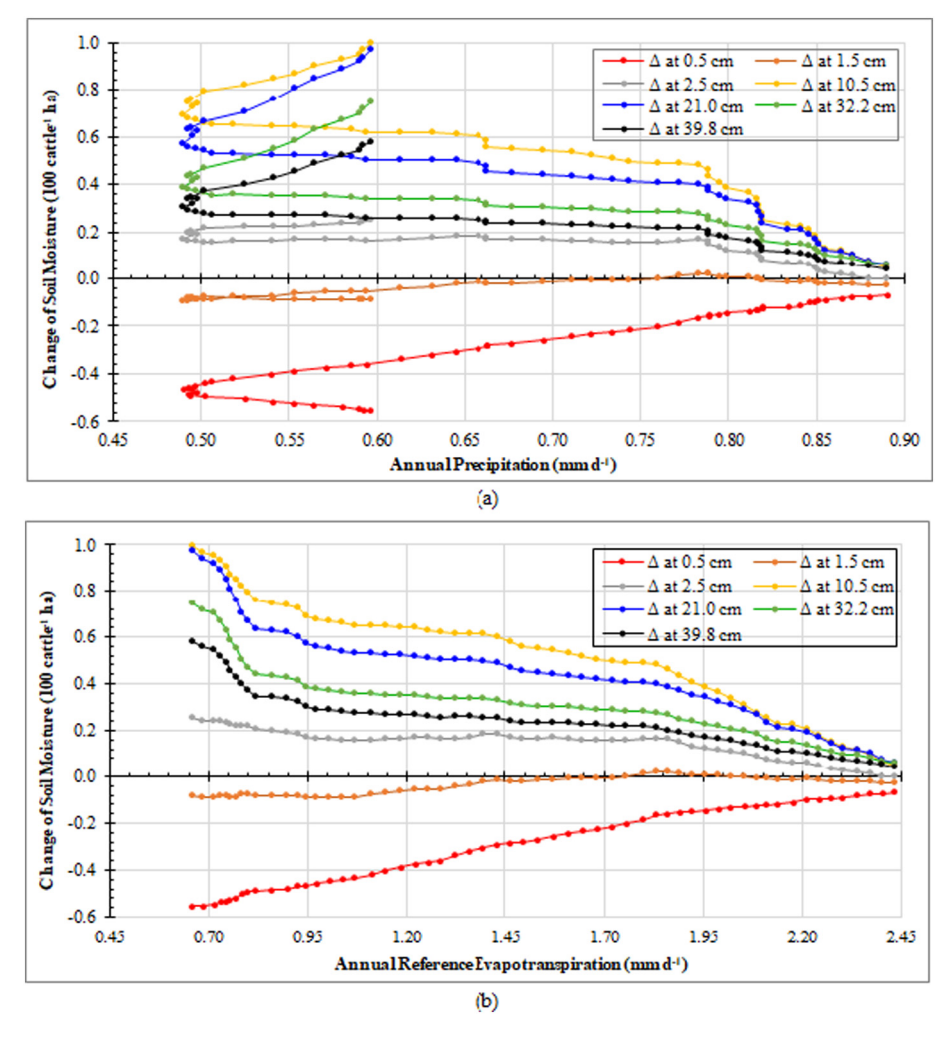


Fig. 9. Average annual change of soil moisture caused by a unit increase of grazing intensity (GI) versus annually standardized: (a) precipitation; and (b) reference evapotranspiration. For a given year of 1960 to 2017, the change for a given day was computed as the soil moisture for GI = 4.0 cattle  $ha^{-1}$  minus the soil moisture for GI = 0.0; and then the arithmetic average of the computed daily changes was divided by 4.0 to get the y-axis value of this year. The x-axis value was standardized as the ratio of the annual total to the corresponding number of days, leading to a units of mm  $d^{-1}$ , for the convenience of plotting.

be comparable at these two locations. However, the precipitation, which is the sole source of soil water, could have a large spatial heterogeneity (Gao et al., 2017); that is, the precipitation amount and/or timing at the climate station might be somewhat different from that at the measurement site, which can be inferenced from Fig. 6: the soil moistures increased or peaked on some days with no precipitation but decreased or troughed on some other days with precipitation. This is also true for the other three calibration years of 2014, 2016, and 2017. Nevertheless, the model is sufficiently calibrated for simulating the long-term average and variability of soil moistures, as indicated by the performance statistics listed in Table 4.

The amount and variability of precipitation during the grazing season (i.e., from May 20 to September 30) are greater than those during the nongrazing season (Fig. 8a), while the rate and variability of reference evapotranspiration during the grazing season are also larger than those during the nongrazing season (Fig. 8b). During the grazing season, the higher soil moistures can be attributed to the larger precipitation, while their smaller variability is likely because the increasing precipitation is proportionally offset by the increasing evapotranspiration, and vice versa. In contrast, during the nongrazing season, the overall lower soil moistures are due to the smaller precipitation as well as snowpack accumulation and soil freezing in November to mid-February. From late February to beginning April, the snowpack starts melting while the frost soils begin thawing, resulting in the pulses of soil moistures (Fig. 8). The multiple pulses, which synchronize with the melting-thawing-freezing

cycles, lead to the larger intraday variability of soil moistures during the nongrazing season.

The top 30-cm soils lose water to both evaporation and transpiration (Wang, 2015; Pedram et al., 2018). The efficient heat exchange between this layer of soils and the ambient atmosphere can quickly vaporize the soil water that is replenished from a precipitation event once it ends, while the richer roots in this layer of soils (Fig. 3) can effectively uptake the soil water for transpiration. As a result, although the highly permeable soils (Fig. 2) may be rapidly replenished by infiltration from precipitation, they can be quickly dried up by evaporation and transpiration. This explains why this layer of soils has a wider range of moistures than the below-40-cm soils (Figs. 7 and 8). The moistures of the 30- to 40-cm soils have a widest range probably because of the increased rate of downward seepage into the lower soil layer, which is more permeable than the upper soil layer (Fig. 2b and Table 3). Such vertical distributions of soil moistures are also true for the nongrazing season, which may be due to the melting-thawing-freezing cycles of snowpack and soils as well as the soil water evaporation and seepage patterns, which are similar for both seasons. Our soil moisture vertical distributions are consistent with those reported by previous studies (Kurc and Small, 2007; Pereyra et al., 2017).

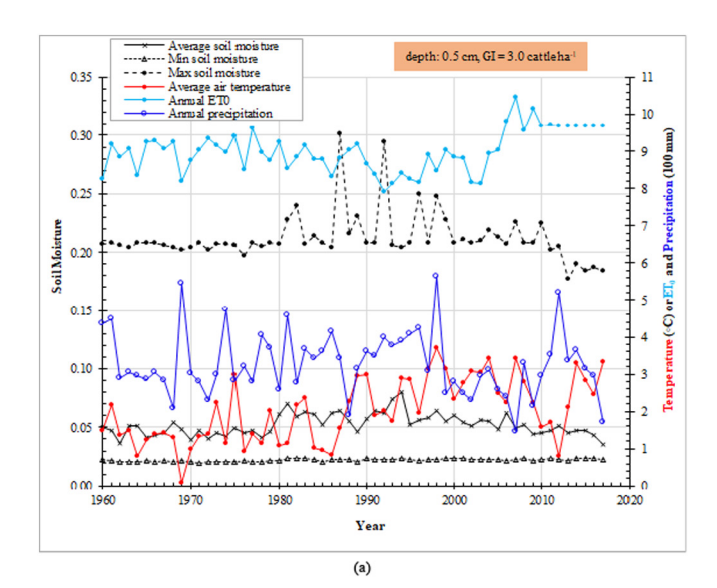
Grazing reduces the aboveground biomass and grass leaf areas. On the one hand, this can make more bare ground surfaces be directly exposed to solar radiations, increasing the soil water evaporation from, and reducing the soil moisture of, the top 1.5-cm soils (Fig. 9). On the other hand, once a top dry soil layer is formed, it will retard the beneath moist soils to be further dried up (Wang, 2015). Also, the grazing removal of grass stems and leaves will reduce transpiration rate and thus water uptake from the rootzone. These two effects are added up to result in higher moistures of the below-1.5-cm soils. As expected, the grazing effects on soil moisture increase with grazing intensity, plateauing at a threshold of 4.0 cattle ha<sup>-1</sup> (Fig. 8). Once the grazing intensity is greater than this threshold, no more grass stems and leaves may be available for grazing to further reduce transpiration. For years with an annual precipitation of less than 220 mm, if most of the precipitation can be quickly evaporated due to a very large ET<sub>0</sub>, the grazing effects will increase with increase of precipitation; otherwise, the grazing effects will decrease with increase of precipitation; for years with an annual precipitation of more than 220 mm, the grazing effects monophonically decrease with increase of precipitation (Fig. 9a).

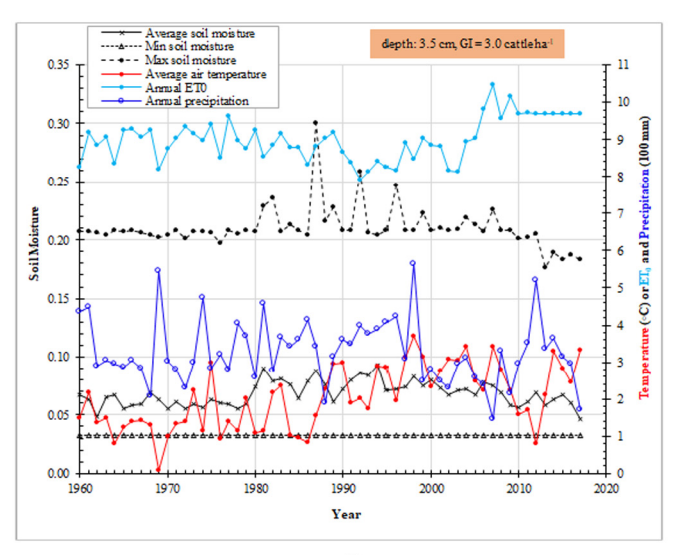
On a day when  $\mathrm{ET}_0$  is not much larger than precipitation, the grazing impact tends to be positively related to the area of exposed bare surfaces, which is smaller for a lower than a higher GI. A smaller area of exposed bare surfaces can reduce heat exchange and decelerate water evaporation from the surface ponding reservoir, providing a relatively favorable condition for infiltration to replenish soil water: the larger the precipitation, the more the infiltration, and vice versa. In contrast, a greater area of exposed bare surfaces will facilitate water evaporation from the surface ponding reservoir, making most precipitation be lost to evaporation without a chance for infiltration to replenish soil moisture. As a result, the transpiration will be greatly decreased, while the evaporation can be largely increased. The absolute soil moisture difference between grazing and nongrazing situations will become larger as increasing precipitation.

On a day when  $ET_0$  is much larger than precipitation, most precipitation water may be evaporated before it can infiltrate into ground to replenish soil moisture (Charbeneau, 2000). As precipitation increases, an increasing percentage of  $ET_0$  will be supplied by direct evaporation of intercepted precipitation, reducing soil water loss to evaporation and transpiration. Because the interception tends to increase with precipitation, the soil moisture change from grazing decreases with increase of precipitation. This is also true for the years with an annual precipitation of larger than 200 mm, when most precipitation is likely to be directly evaporated to meet  $ET_0$  rather than infiltrates into ground to replenish soil moisture. Moreover, as  $ET_0$  increases, more precipitation tends to be directly evaporated, leading to the monophonically negative relationships between soil moisture change from grazing and  $ET_0$  (Fig. 9b).

For semiarid steppe grasslands such as the Balagaer River watershed, wind erosion is always a serious concern (Wang et al., 2014; Potter, 2019). This is particularly true in early spring, when snowpack disappears, wind speed is high, and vegetation cover has not been fully established yet. Thus, the pulsing soil moistures from late February to beginning April (Fig. 8) are vital for preventing fertile fine particles from being eroded by wind. Once the fine particles are detached by wind, they would be suspended in air and blown to a very long distance, possibly forming dust storms (Duan et al., 2011). Wang et al. (2014) and Potter (2019) found that wind erosion would be manageable if the topsoil moisture is greater than 0.15 in the study watershed. Across the 58 assessment years, the number of days with a daily soil moisture of greater than 0.15 in March and April would be reduced by 3 and 24 d for GI = 3.0 and 4.0 cattle ha<sup>-1</sup>, respectively; and the grazing season by 9 and 78 d for these two GIs, respectively. Although grasses are growing in the grazing season, the grazing removal of grass stems and leaves by more than 4.0 cattle ha<sup>-1</sup> will make more bare soils be exposed and susceptible to wind erosion. Thus, a grazing intensity of up to 3.0 cattle seems optimal for our study grassland.

Regardless of the grazing intensities and/or soil depths, for the historical climatic conditions, the annual minimum daily soil moistures would be visually invariant, whereas the annual maximum daily and the average annual soil moistures would slightly vary from 1960 to 1980, largely fluctuate from 1980 to 2000, and tend to decrease from 2000 onward (Fig. 10). However, for a given grazing intensity, the soil





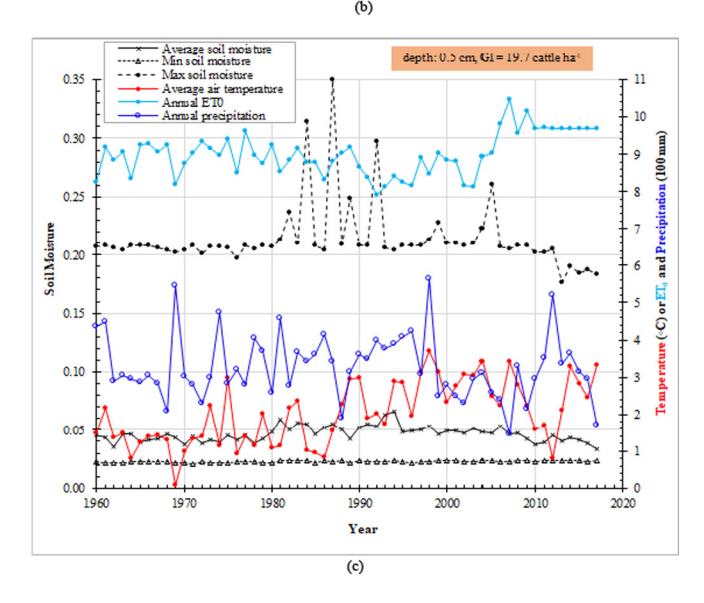


**Fig. 10.** The timeseries plots of the soil moistures at: (a) soil depth of 0.5 cm and grazing intensity (GI) of 3.0 cattle ha<sup>-1</sup>; (b) soil depth of 3.5 cm and GI = 3.0 cattle ha<sup>-1</sup>; and (c) soil depth of 0.5 cm and GI = 19.7 cattle ha<sup>-1</sup>. The results are for the historical (i.e., 1960 to 2017) climatic conditions that are surrogated by average annual air temperature, annual reference evapotranspiration (ET<sub>0</sub>), and annual precipitation.

moisture fluctuations at a shallower depth are larger than those at a deeper depth (e.g., Fig. 10a versus Fig. 10b), whereas for a given depth, the soil moisture fluctuations if GI  $\leq$  3.0 cattle  $ha^{-1}$  are less than those if GI  $\geq$  4.0 cattle  $ha^{-1}$  (e.g., Fig. 10a versus Fig. 10c). In principle, the topsoil moistures are closely related to the amounts and temporal distributions of precipitation and ET $_0$  (Fig. 9). Besides air temperature, several other climatic variables, namely wind speed, solar radiation, humidity, and vapor pressure deficit, also affect ET $_0$ ; thus, the soil moisture fluctuations are not positively correlated with air temperature. The decreasing trend in the post-2000 soil moistures can be attributed to the increasing ET $_0$  and decreasing precipitation.

As a logical generalization to the whole semiarid Eurasian steppe grasslands, soil moistures synchronically fluctuate with patterns of rainfall, atmospheric evaporation demand, snow accumulating and melting, and soil freezing and thawing. The predicted reducing snowfall and snowpack accumulation in winter from climate change would dimmish soil moisture pulses in early spring, increasing the susceptibility of fertile fine soil particles to wind erosion while deteriorating the sustainability and resilience of grassland ecosystem and commodity. It is imperative to practice livestock grazing below a threshold grazing intensity (e.g., around 3.0 cattle ha<sup>-1</sup>); otherwise the topsoil moistures would be lowered and grass stems and leaves could be removed too much to protect surface soils as a vegetation cover, increasing the risk of grassland degradation and even desertification.

#### 6. Conclusions

This study formulated and parameterized a SWAP model for simulating long-term responses of soil moistures to climate variability and livestock grazing in the Balagaer River watershed, a typical Eurasian steppe grassland. The model was calibrated using the measured daily soil temperatures and soil moistures at multiple depths to be sufficiently accurate for the simulation purpose of this study. For the study grassland, the daily soil moistures were predicted to vary from 0.02 to 0.38, with a smaller value at a shallower than a deeper depth. The soil moistures around the 30-cm depth had a largest mean and a widest range. Regardless of the depths, the soil moistures pulsed in beginning March and plateaued from May to September. Livestock grazing was precited to decrease the top 1.5-cm soil moistures but increase the moistures of the beneath soils. The optimal grazing intensity was determined to be around 3.0 cattle  $ha^{-1}$ , above which the number of days with a topsoil moisture of greater than 0.15 will be phenomenally reduced. The grazing impacts on soil moisture were found to monophonically decrease with increase of reference evapotranspiration and annual precipitation when it is larger than 220 mm. For the years with an annual precipitation of less than 220 mm, the grazing impacts could either increase or decrease with increase of precipitation, depending on the relative magnitude of daily reference evapotranspiration. In generalization, across the semiarid Eurasian ecoregion, it is imperative to practice pasturing below a threshold grazing intensity to confront land degradation being intensified by climate change.

## CRediT authorship contribution statement

Xixi Wang parameterized the model, did the analyses, and wrote the paper.

Ruzhong Gao collected and preprocessed the data, formulated the scenarios, and wrote portion of the Discussion section.

Xiaomin Yang prepared the model inputs and did the simulations.

## **Declaration of competing interest**

The authors declare that they have no known competing financial interests or personal relationships that could have appeared to influence the work reported in this paper.

## Acknowledgements

This study was financially supported by the following contracts: U.S. National Science Foundation (NSF) International Research Experiences for Students (IRES) (# 1654957); and National Natural Science Foundation of China (NSFC) (# 51969022). This study advanced the preliminary results of the NFS-IRES student participants, including Alston D. Chereskin, Devrick L. Johnson, Nicholas M. Potter, Zachary C. Landis, Robert S. McElhinny Jr., Alexander J. Leonard, Angela L. Tsao, Lillian K.W. Michaud, Parker M. Bartz, and Along Zhang.

## References

- AHDB, 2020. Calculating dry matter intakes for rotational grazing of cattle. Retrieved December 6, 2020, from. https://ahdb.org.uk/knowledge-library/calculating-dry-matter-intakes-for-rotational-grazing-of-cattle.
- Allen, R.G., Wright, M.E., Burman, R.D., 1989. Operational estimates of evapotranspiration. Agron. J. 81, 650–662.
- Allen, R.G., Pereira, L.S., Raes, D., Smith, M., 1998. Crop evapotranspiration: guidelines for computing crop water requirements. Irrigation and Drainage Paper 56. FAO, Rome, Italy, p. 300.
- Ashby, M., Dolman, A.J., Kabat, P., Moors, E.J., Ogink-Hendriks, M.J., 1996. SWAPS version 1.0 Technical Reference Manual: Technical Document 42. Winland Staring Center, Wageningen, UK.
- Bartholomeus, R.P., Witte, J.P.M., van Bodegom, P.M., van Dam, J.C., Aerts, R., 2008. Critical soil conditions for oxygen stress to plant roots: sustituting the Feddes-function by a process-based model. J. Hydrol. 360. 147–165.
- Boogaard, H.L., de Wit, A.J.W., te Roller, J.A., van Diepen, C.A., Rötter, R.P., Cabrera, J.M.C.A., van Laar, H.H., 2014. WOFOST Control Centre 2.1 and WOFOST 7.1.7. Alterra, Wageningen University & Research Centre, Wageningen, The Netherlands.
- Charbeneau, R.J., 2000. Groundwater Hydraulics and Pollutant Transport. Waveland Press, Inc., Long Grove, IL.
- Chen, S., Bai, Y., Zhang, L., Han, X., 2005. Comparing physiological responses of two dominant grass species to nitrogen addition in Xilin River Basin of China. Environ. Exp. Bot. 53, 65–75.
- Cheng, Z., Meng, J., Wang, Y., 2016. Improving spring maize yield estimation at field scale by assimilating time-series HJ-1 CCD data into the WOFOST model using a new method with fast algorithms. Remote Sens. 8 (4), 1–22.
- CMIC, 2020. National Meteorological Data. from. http://www.nmic.gov.cn/web/index.
- Doherty, J., 2004. PEST: Model-Independent Parameter Estimation User Manual. 5th ed. Watermark Numerical Computing, Brisbane, Australia.
- Duan, L., Liu, T., Wang, X., Wang, G., Ma, L., Luo, Y., 2011. Spatio-temporal variations in soil moisture and physicochemical properties of a typical semiarid sand-meadow-desert landscape as influenced by land use. Hydrol. Earth Syst. Sci. 15 (6), 1865–1877.
- Feddes, R.A., Kowalik, P.J., Zaradny, H., 1978. Simulation of field wate use and crop yield. Simulation Monographs, p. 189 Wageningen, The Netherlands.
- Gao, R., Li, F., Wang, X., Liu, T., Du, D., Bai, Y., 2017. Spatiotemporal variations of precipitation across the Mongolian Plateau of China over the past half century. Atmos. Res. 193, 204–215.
- van Genuvhten, M.T., 1980. A closed-form equation for predicting the hydraulic conductivity of unsaturated soils. Soil Sci. Soc. Am. J. 44, 892–898.
- Hack-ten Broeke, M.J.D., Kroes, J.G., Bartholomeus, R.P., van Dam, J.C., de Wilt, A.J.W., Supit, I., Walvoort, D.J.J., van Bakel, P.J.T., Ruijtenberg, R., 2016. Quantification of the impact of hydrology on agricultural production as a result of too dry, too wet or too saline conditions. Soil 2, 391–402.
- Hillel, D., 1980. Fundamentals of Soil Physics. CA, Academic Press, San Diego.
- Huxman, T.E., Snyder, K.A., Tissue, D., Leffler, A.J., Ogle, K., Pockman, W.T., Sandquist, D.R., Potts, D.L., Schwinning, S., 2004. Precipitation pulses and carbon fluxes in semiarid and arid ecosystems. Oecologia 141, 254–268.
- van Ittersum, M.K., Leffelaar, P.A., van Keulen, H., Kropff, M.J., Bastiaans, L., Goudriaan, J., 2003. On approaches and applications of the Wageningen crop models. Eur. J. Agron. 18, 201–234.
- de Jong van Lier, Q., van Dam, J.C., Metselaar, K., de Jong, R., Duijnisveld, W.H.M., 2008. Macroscopic root water uptake distribution using a matric flux potential approach. Vadose Zone J. 7, 1065–1078.
- Kroes, J.G., 2020. In: Wang, X. (Ed.), Personal Email Communication: Modeling Grass Growth.
- Kroes, J.G., van Dam, J.C., Bartholomeus, R.P., Groenendijk, P., Heinen, M., Hendriks, R.F.A., Mulder, H.M., Supit, I., van Walsum, P.E.V., 2017. SWAP Version 4: Theory Description and User Manual. Wageningen Environmental Research, Wageningen, The Netherlands.
- Kurc, S.A., Small, E.E., 2007. Soil moisture variations and ecosystem-scale fluxes of water and carbon in semiarid grassland and shrubland. Water Resour. Res. 43, W06416.
- Luo, Y., Liu, T., Wang, X., Duan, L., 2012. Influences of landform as a confounding variable on SOM-NDVI association in semiarid Ordos Plateau. J. Arid Land 4 (4), 450–456.
- Luo, Y., Wang, X., Li, F., Gao, R., Duan, L., Liu, T., 2014. Responses of grass production to precipitation in a mid-latitude typical steppe watershed. Trans. ASABE 57 (6), 1595–1610.
- Ma, Y., Feng, S., Huo, Z., Song, X., 2011. Application of the SWAP model to simulate the field water cycle under deficit irrigation in Beijing, China. Math. Comput. Model. 54, 1044–1052.

- Maas, E.V., Hoffman, G.J., 1977. Crop silt tolerance-current assessment. J. Irrig. Drain. 103, 115-134
- METER Group, I, 2020. Measure the Soil-Plant-Atmosphere Continuum. Retrieved December 29, 2020, from. https://www.metergroup.com/environment/.
- Monteith, J.L., 1965. Evaporation and the environment. In: Fogg, G.E. (Ed.), The State and Movement of Water in Living Organisms. Cambridge University Press, New York, NY, pp. 205–234.
- Mualem, Y., 1976. A new model for predicting the hydraulic conductivity of unsaturated porous media. Water Resour. Res. 12, 513–522.
- Neumann, I.B., Wigen, E., 2013. The importance of the Eurasian steppe to the study of international relations. J. Int. Relat. Dev. 16, 311–330.
- Pedram, S., Wang, X., Liu, T., Duan, L., 2018. Simulated dynamics of soil water and pore vapor in a semiarid sandy ecosystem. J. Arid Environ. 151, 58–82.
- Penman, H.L., 1948. Natural evaporation from open water, bare soil, and grass. Proc. R. Soc. Lond. 193, 120–146.
- Pereyra, D.A., Bucci, S.J., Arias, N.S., Ciano, N., Cristiano, P.M., Goldstein, G., Scholz, F.G., 2017. Grazing increases evapotranspiration without the cost oflowering soil water storages in arid ecosystems. Ecohydrology 10, e1850.
- Philip, J.R., de Vries, D.A., 1957. Moisture movement in porous materials under temperature gradients. Trans. Am. Geophys. Union 38, 222–232.
- Potter, N.M., 2019. Measuring and Modeling Bare Desert Wind Erosion From Steppe Grassland of Northern China as Affected by Soil Moisture and Climate. (M.S.). Old Dominion University.
- Saxton, K.E., Rawls, W.J., 2006. Soil water characteristic estimates by texture and organic matter for hydrologic solutions. Soil Sci. Soc. Am. J. 70, 1569–1578.
- Schaap, M.G., van Genuchten, M.Th., 2006. Modified mualem-van Genuchten formulation for improved description of the hydraulic conductivity near saturation. Vadose Zone J. 5, 27–34.
- Shiyomi, M., Akiyama, T., Wang, S., Yiruhan, Ailikun, Hori, Y., Chen, Z., Yasuda, T., Kawamura, K., Yamamura, Y., 2011. A grassland ecosystem model of the Xilingol steppe, Inner Mongolia, China. Ecol. Model. 222, 2073–2083.
- Singh, J.S., Milchunas, D.G., Lauenroth, W.K., 1998. Soil water dynamics and vegetation patterns in a semiarid grassland. Plant Ecol. 134, 77–89.

- USDA-NRCS, 2020. Animal Unit Equivalent Texas: Domestic Livestock, Native Wildlife, and Exotic Wildlife. Retrieved December 6, 2020, from. https://www.nrcs.usda.gov/Internet/FSE\_DOCUMENTS/nrcs144p2\_002433.pdf.
- Vanderborght, J., Fetzer, T., Mosthaf, K., Smits, K.M., Helmig, R., 2017. Heat and water transport in soils and across thesoil-atmosphere interface: 1. Theory and different modelconcepts. Water Resour. Res. 53, 1057-1079.
- de Vries, D.A., 1963. Thermal properties of soils. In: van Wijk, W.R. (Ed.), Physics of Plant Environment. North-Holland Publishing Company, Amsterdam, Netherlands.
- Wang, X., 2015. Vapor flow resistance of dry soil layer to soil water evaporation in arid environment: an overview. Water 7 (8), 4552–4574.
- Wang, X., Melesse, A.M., 2005. Evaluation of the SWAT model's snowmelt hydrology in a northwestern Minnesota watershed. Trans. ASAE 48 (4), 1359–1376.
- Wang, Y., Zhou, G., 2012. Light use efficiency over two temperate steppes in Inner Mongolia. China. PLoS One 7 (8), e43614.
- Wang, X., Yang, W., Melesse, A.M., 2008. Using hydrologic equivalent wetland concept within SWAT to estimate streamflow in watersheds with numerous wetlands. Trans. ASABE 51 (1), 55–72.
- Wang, X., Liu, T., Yang, W., 2012. Development of a robust runoff-prediction model by fusing the rational equation and a modified SCS-CN method. Hydrol. Sci. J. 57 (6), 1118–1140.
- Wang, X., Liu, T., Li, F., Gao, R., Yang, X., Duan, L., Luo, Y., Li, R., 2014. Simulated soil erosion from a semiarid typical steppe watershed using an integrated aeolian and fluvial prediction model. Hydrol. Process. 28 (2), 325–340.
- Wang, Z., Ji, L., Hou, X., Schellenberg, M.P., 2016. Soil respiration in semiarid temperate grasslands under various land management. PLoS One 11 (1), e0147987.
- Wang, Z., Wan, X., Tian, M., Wang, X., Chen, J., Chen, X., Chang, S., Hou, F., 2020. Grazing season alters soil respiration in a semiarid grassland on the Loess Plateau. Nutr. Cycl. Agroecosyst. 118, 177–191.
- de Wit, A., Duveiller, G., Defourny, P., 2012. Estimating regional winter wheat yield with WOFOST through the assimilation of green area index retrieved from MODIS observations. Agric. For. Meteorol. 164, 39–52.
- Yang, X., 2014. Hydro-Climate Temporaral Variations and Their Influences on Net Primary Production in a Eurasian Steppe Watershed. (M.S.). Old Dominion University.